The Electronic Device with Resistance Switching Behavior based on Different Mechanisms

by

Baizhou Zhang

A thesis

presented to the University of Waterloo

in fulfillment of the

thesis requirement for the degree of

Master of Applied Science

in

Mechanical and Mechatronics Engineering

Waterloo, Ontario, Canada, 2023

©Baizhou Zhang 2023

Author's Declaration

I hereby declare that I am the sole author of this thesis. This is a true copy of the thesis, including any required final revisions, as accepted by my examiners.

I understand that my thesis may be made electronically available to the public.

Abstract

Due to the limitations of materials and structures, the performance of the von Neumann structure of traditional computers cannot meet the needs of today's people. The development of new electronic devices is the most effective way to improve the performance of computers. Devices with resistive switching behavior can realize simultaneous operating data storage and processing, which greatly saves the space required for device integration and reduces energy consumption at the same time. These advantages provide it with huge potential in advanced technology fields such as machine learning and neuromorphic computing. However, there are still challenges such as stability, miniaturization and working environment before this device realized its business purpose. In this thesis, memristor with rectifying effect is fabricated successfully, and its possible applications of neuromorphic computing and logic operations are discussed. In addition, two different methods were used to prepare phase-change materials, which are expected to be fabricated into phase-change memories.

Acknowledgments

This thesis would have been impossible without the guidance and encouragements of several people. I would like to express my deepest gratitude to my supervisor, Professor Yimin Wu, for his continuous support and valuable insights throughout my master's at University of Waterloo.

I would like to thank the rest of my thesis committee: Professor Kevin Musselman and Professor Yue Hu, for their insightful comments and encouragement.

I would also like to thank Dr. Tao Guo for providing valuable suggestions and directions during my research.

I would also like to extend my appreciation to my lab colleagues Yongzan Zhou, Zuolong Chen, Youchao Teng, Siyan Lu and Wei Wei, who helped me a lot with multiple characterization.

Last but not least, I would also like to thank my family and friends who supported me unconditionally all the time.

Table of Contents

Author's Declaration ii

Abstract iii

Acknowledgements iv

List of figures vii

1. Introduction 1

1.1 Electronic device 1

1.1.1 Current electronic device 1

1.1.2 NRAM 2

1.2 Memristor 3

1.2.1 Development of memristor 3

1.2.2 Application of memristor in neuromorphic computing 5

1.3 Switching behavior 6

1.4 Vacancy migration & Multi-state memristor 8

1.5 ZnO memristor 10

1.6 Phase change memory 12

1.7 Sb_2Te_3 phase change material and its fabricating methods 14

1.8 Summary 16

2. Asymmetric-resistive-switching device with reconfigurable synaptic functions for logic operations 17

2.1 Overview 17

2.2 Experiments and Methods 17

2.2.1 Device fabrication 17

2.2.2 Material and device characterization 17

2.3 Results and Discussion 18

2.3.1 Material characterization 18

2.3.2 Electronic performance 19

2.3.3 The mechanism of ARS 21

2.3.4 Demonstration of logic operation based on multi-state memristor 24
2.4 Summary 25
3. Sb_2Te_3 phase change crystal material preparation 27
3.1 Overview 27
3.2 Experiment and Methods..... 27
3.2.1 CVD method..... 27
3.2.2 CVT method 28
3.2.3 Material characterization 28
3.3 Results and Discussion 28
3.3.1 Material characterization for Sb2Te3 deposited on wafer 28
3.3.2 Material characterization for Sb2Te3 prepared by CVT 29
3.4 Summary 31
4. Conclusions and future work..... 32
References 33

List of figures

Figure 1.1 A schematic diagram of the memristor applied to the neural unit and artificial synapses [2]. Adapted from ACS Applied Bio Materials journal with permission.

Figure 1.2 The relationships between 4 circuit components: Resistor, capacitor, inductor and memristor [24]. Adapted from Nature journal with permission.

Figure 1.3 The layered structure of the principal non-volatile RAMs: (a) FeRAM (ferroelectric RAM); (b) MRAM (magnetic RAM); (c) PCRAM (phase-change RAM) and (d) RRAM (resistive RAM) [47]. Adapted from Materials journal with permission.

Figure 1.4 I-V curve & electrochemical reaction inside the active layer of the memristor based on silver conductive filament [48]. Adapted from Advanced Materials journal with permission

Figure 1.5 (a) Vertical structure. (b) Parallel structure. (c) Cross-bar structure [74]. Adapted from Interdisciplinary Research for Printing and Packaging with permission.

Figure 1.6 (a) Speed versus price per GB of various memory and storage [107]. (b) 3D Xpoint setup[102]. (c) Phase change principle [108]. Figure a. and Figure c. adapted from IEEE journal and Nature journal with permission, respectively.

Figure 1.7 The important classes of phase-change materials (PCMs) are found in the Ge–Sb–Te ternary diagram [131]. Adapted from Nature journal with permission.

Figure 2.1 (a) The SEM image & EDS results of ZnO. (b) The SEM image & EDS results of ITO. (c) XRD result of ZnO. (d) & (e) XPS result of ZnO. (f) UPS result of ZnO.

Figure 2.2 (a) I-V curves of the device with ARS, in which the red curve shows the asymmetric Reset/Set process and the blue curve indicates long-term stability. (b) Conductance of device at HRS/LRS under positive/negative of the same amplitude voltage. (c) and (d) Potentiation/depression properties of the device under positive/negative electronic pulses, whose duration was 100 ms.

Figure 2.3 (a) The fitting line of ln(I) vs. E1/2 for the device at HRS. (b) The fitting line of ln(I/T2) vs. 1000/T for the device at HRS. (c) Schematic diagram of energy band for the device at HRS. (d) The fitting line of log(I) vs. log(V) for the device at LRS under positive voltage. (e) The fitting of log(|I|) vs. log(|V|) for the device at LRS under negative voltage. (f) Schematic diagram of energy band for the device at LRS.

Figure 2.4 (a) Schematic diagram of the device applied in logic computing. (b) AND & OR logic truth table. (c) A demonstration of OR logical operation. (d) A demonstration of AND logical operation. The dotted line in Figure 2.4 c & d is the threshold 40 nS.

Figure 3.1 (a-d) The SEM image of the Sb_2Te_3 deposit on the wafer. (e-h) The EDS results and composition mapping of Sb_2Te_3.

Figure 3.2 (a) The image of Sb_2Te_3 crystal prepared in the ampoule tube. (b) & (c) The SEM image of Sb_2Te_3 crystal. (d-g) EDS results and composition mapping of Sb_2Te_3 crystal.

Figure 3.4 (a) & (b) Mechanical exfoliate crystal onto the wafer. (c) & (d) Mechanical exfoliate crystal onto the tape.

1. Introduction

1.1 Electronic device

1.1.1 Current electronic device

With the rapid development of science and technology, new multifunctional electronic devices are also constantly developing [1]. For applications with different functions depending on different environments, people develop multiple methods to control the performance changes of the devices. Zhou *et al*. studied the use of water to induce electrical transitions in electronic devices [1]. Sun *et al.* also changed the concentration of ionic liquid to affect the proton exchange of graphite in electronic devices, as shown in Figure 1.1, they not only control the device's performance, but also realized the application in artificial synapse [2]. Light can also regulate the functions of electronic devices. Wang *et al.* used different light intensities to achieve the purpose of gathering and dispersing electrons, thereby changing the physical properties of the device such as the potential barrier [3]. It can be found that researchers try to use various methods to adjust the functions of electronic devices, which provides a wide range of work environments for electronic devices.

Although the vigorous development of electronic technology has promoted the rapid progress of society, the huge increase in power consumption runs counter to the energy saving and emission reduction, which is praise highly around the world today. To save energy, reduce power consumption and greenhouse gas emissions, people also began to think about how to achieve low energy input and good output performance of devices, meanwhile reducing waste of energy and environmental impact in the operation and manufacturing processes. Researchers optimize electronic devices through software analysis, structural design, and material properties. Djokic *et al.* analyzed the working efficiency of modern low-voltage electronic components in an under-voltage environment and proposed a feasible efficiency improvement scheme [4], however, the exchange frequency between systems has increased, which has caused another form of energy waste [4]. Through the topology of the original transformer structure, Alishah *et al.* realized the upgrade of the device [5],compared with other devices of the same type, this device achieves lower voltage drop and power loss because it integrates fewer switches [5].

Guo *et al.* developed a new type of environmentally friendly materials based rechargeable battery, while having high energy density and long working life to improve performance [6].

1.1.2 NRAM

Thanks to the development of electronic devices in various aspects and the rise of deep learning, a new computing method, neural network calculations can be realized, which is similar to the human-brain that can store and process information at same time. However, limited by the traditional Von Neumann structure in computers, the computational energy efficiency is low [7]. Non-volatile random access memory (NRAM), as a research hotspot in the field of low-power, high-performance electronic devices, provides an electronic component with both storage and computing capabilities. NRAM usually has multiple electrical states, which can be affected by external stimuli or internal interface changes. Compared to traditional memory, it has advantages of low energy consumption[8][9], fast switching speed [10][11], high integration [12][13], and long working life [14][15]. Many kinds of NRAM were widely studied for performance improvement. Hwang *et al.* reduced the contact resistance of the device by reducing the diameter of the nanowire to reduce its power consumption [16]. In the study of aluminum nitride, Lin *et al.* found that materials with different crystal phases have different thermal stability and power consumption [17]. Cho *et al.* analyzed the crystallization kinetics of phase change materials and found the effect of doping concentration in the material on device stability and switching speed [18]. Studies have found that Li_xSiOy also has excellent stability at high temperatures, fast switching speed, and good durability [19]. Guo *et al.* designed devices at the nanometer scale and achieved ultra-high integration density, but the devices lack stability at high temperatures [20]. It has been reported that the construction of a new structural model of 3-D vertical resistive switching memory with a hexagon-patterned pillar layout, which has greatly improved the integration of devices and the feasibility of the structure has been verified by simulation [21]. Nomura *et al.* respectively verified that NRAM based on different materials still had high stability at high temperatures and maintained a surprising lifetime [22][23]. NRAM has broad, superior performance and great potential in neuromorphic computing and high-performance processor applications.

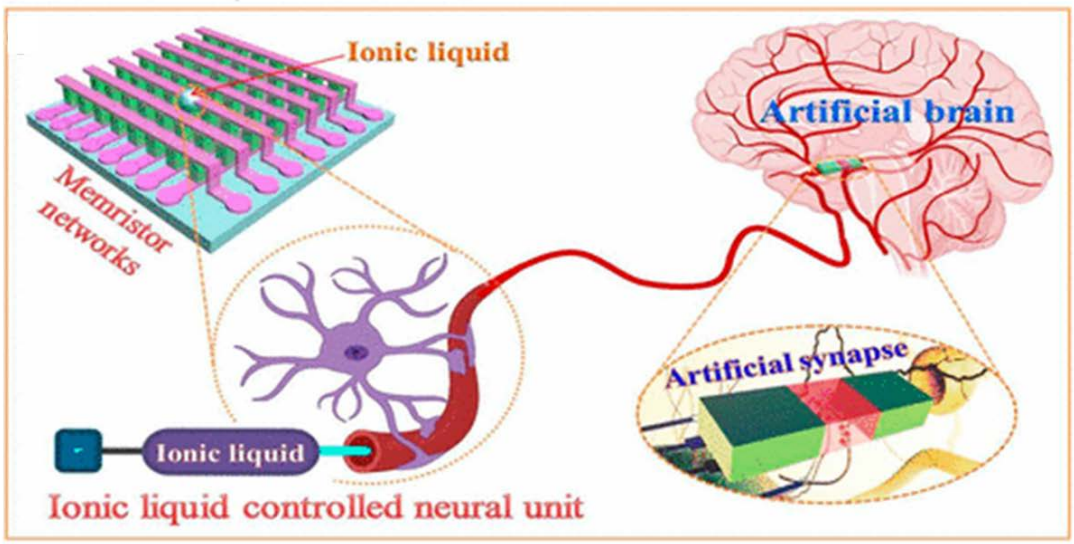


Figure 1.1 A schematic diagram of the memristor applied to the neural unit and artificial synapses [2]. Adapted from ACS Applied Bio Materials journal with permission.

1.2 Memristor

1.2.1 Development of memristor

Since the memristor was first introduced by Dr. Chua in 1971 [24], it has been identified as the 4th basic circuit component after capacitor, resistor and inductor (Figure 1.2). As an iconic representative of NRAM, the memristor has remarkable switching behavior and can be regarded as a combination of memory and resistor. A memristor is a non-linear resistor with memory function whose resistance value can be switched by controlling pulses of applied voltage or current without physical separation between computation and storage [25]. Since the first fabrication of memristor devices by HP in 2008, a variety of materials have been explored to improve device stability, behavior, durability and fabrication methods [26]. As a new type of electronic component, the memristor has attracted extensive attention in recent years. Compared with traditional electronic components such as resistors and transistors, memristors have the advantages of small space, convenient integration, high integration, and non-volatility. They are used in modeling, logic circuit design, information storage, image processing, chaotic circuits, etc.[27-36].

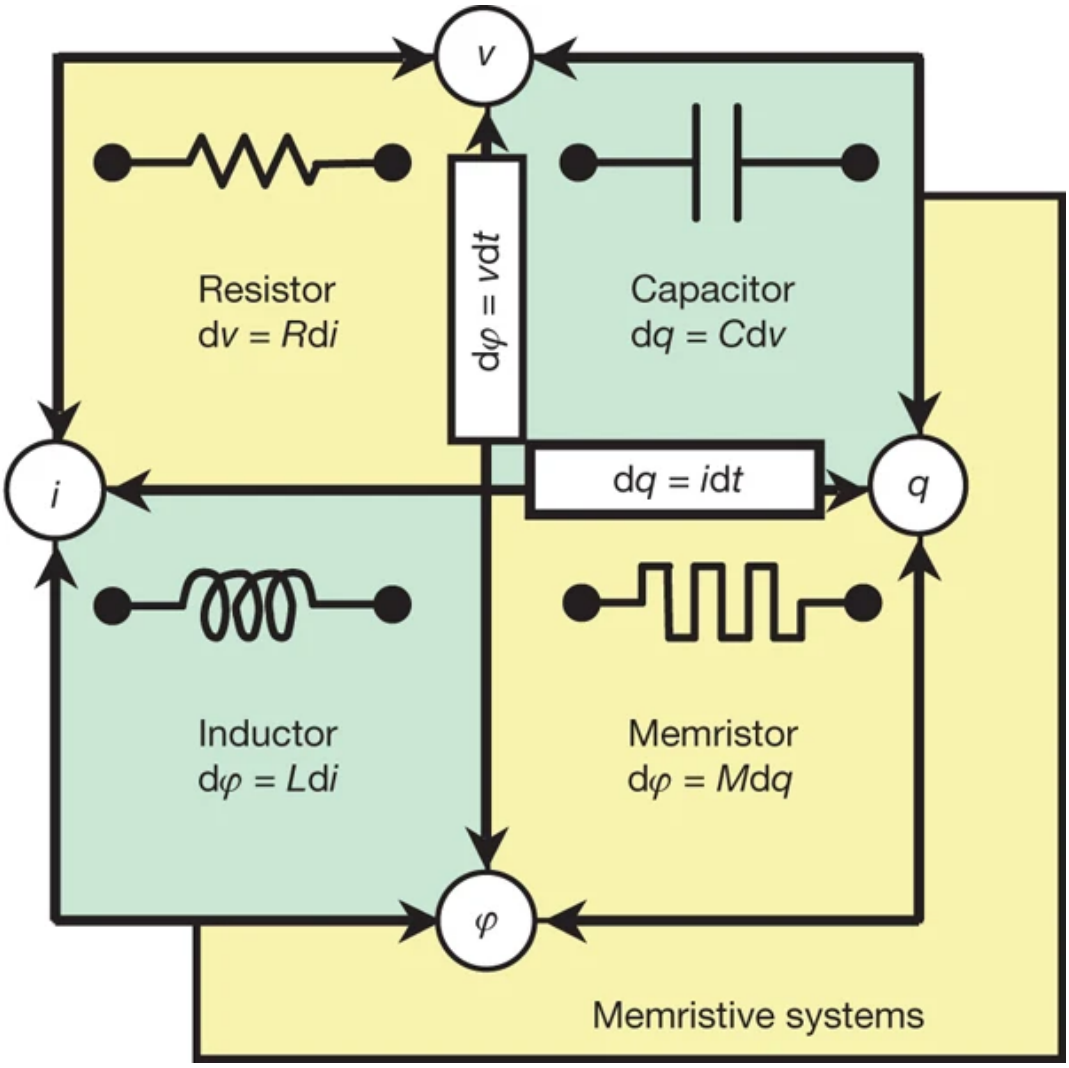


Figure 1.2 The relationships between 4 circuit components: Resistor, capacitor, inductor and memristor [24]. Adapted from Nature journal with permission.

Besides, memristors also show great potential for the development of machine vision at the leading edge of science and technology, because of the temporary memory and real-time processing of sensory data and visual information. To better realize the artificial vision function of memristor, enhancing the memristor response to light stimulation is important. In a related study, Tan *et al.* demonstrated that memristors have a response to external light signals [37]. During the research on organic memristors, Leydecker *et al.* collected resistance changes for different colors of light stimuli and had good stability [39]. Using certain illuminations with different light intensities, the device realizes the perception and storage of light information and has a synaptic-like learning behavior [40]. Zhou *et al.* fabricated a memristor with photoelectric

response based on perovskite materials, which can perform logic operations on optical and electrical signals [41]. In conclusion, memristor can perfectly support artificial vision function, furthermore, memristor-based artificial vision devices can not only realize visual sensing, but also have potential applications in artificial intelligence.

1.2.2 Application of memristor in neuromorphic computing

The human brain can perform specific tasks in complex environments more efficiently than traditional computers, such as data classification and image recognition. The human brain is capable of complex functions, as a result of neurons and synapses that can process information in massive amounts parallelly. There are two important mechanisms in the biological nervous system, which called long-term potentiation (LTP) and long-term depression (LTD). The special resistive switching mechanism of the memristor can realize the complex functions of LTP and LTD [42]. To realize the application of memristors in neural networks, there are some key requirements for the devices. For example, higher resistance is required to achieve low power consumption, high endurance is needed for machine training, a wide resistance range is necessary to have multi-resistance states, devices are required to have low device-to-device variation and resistance stability [43]. Choi *et al.* prepared a new type of device which first used single layer SiGe as the active layer, it has a wide resistance range and realized the multiple resistance states required for neural network simulation calculations [44]. Yan *et al.* successfully increased the resistance switching speed of the device to the nanosecond level in the study of TiO_2, by doping self-assembled Ag nanoclusters. In addition, the memristor has low resistance and low device-device variation [45]. Xia *et al.* reported that the reprogramming and training of memristors in neuromorphic computing required high durability, and the chips are built into interleaved arrays to perform efficient in-memory computations in parallel. Besides, the report also demonstrates that the dynamic interaction of memristors between artificial synapses and neurons enables the network to have the ability of machine learning [46]. The various excellent properties of memristors provide a broad platform for machine learning and neural network simulation, which can bring great progress for human computing analysis.

1.3 Switching behavior

To further improve the performance of resistive switching behavior devices and provide a theoretical basis for their possible applications, the study of the mechanism is necessary and worth exhaustive study. In mainstream research, five mechanisms are generally accepted and verified: vacancy migration, phase transition principle, electrochemical principle, tunneling magneton theory, and ferroelectric theory (Figure 1.3) [47].

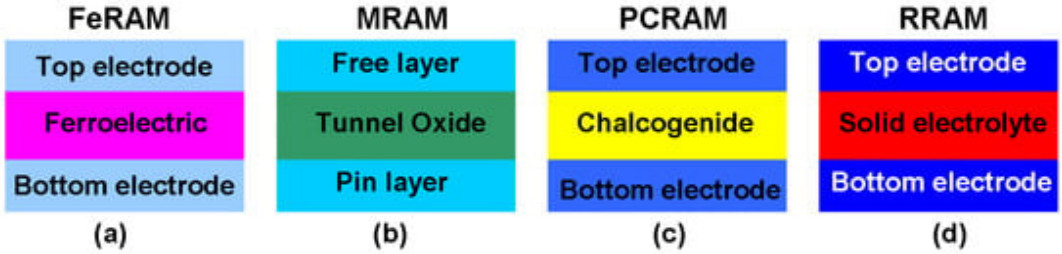


Figure 1.3 The layered structure of the principal non-volatile RAMs: (a) FeRAM (ferroelectric RAM); (b) MRAM (magnetic RAM); (c) PCRAM (phase-change RAM) and (d) RRAM (resistive RAM) [47]. Adapted from Materials journal with permission.

The most common electrochemical principles are based on the formation and disappear of conductive filaments in the functional layers of the device. Due to the advantages of easy regulation of the conductive filaments, the resistive variable memory based on this theory has received extensive attention. In principle, as shown in the Figure 1.4A, the electrode metal undergoes a reduction reaction and transforms into ions which diffuse into the functional layer under applied voltage. These metal ions move under the attraction of the negative electrode, and during the movement process, they interact with the migrating electrons to form metallic filament. This process is exacerbated by increasing the electric field, leading to the formation of metal filaments that grow preferentially along the direction of the negative electrode (Figure 1.4A). After the wire grows to form a metallic filament and contact with the opposing M electrode, the device switches to the ON state (Figure 1.4B). When a sufficient opposite voltage is applied, the wires in the interface are electrochemically dissolved (Figure 1.4C) and reset the memristor to its initial off state (Figure 1.4D).

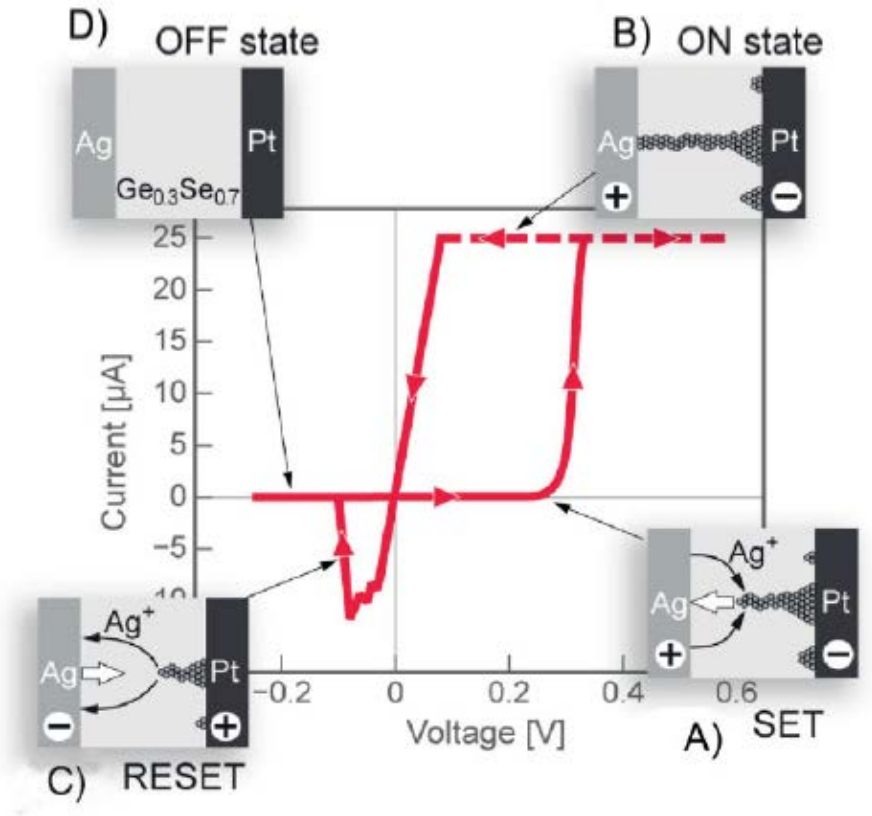


Figure 1.4 I-V curve & electrochemical reaction inside the active layer of the memristor based on silver conductive filament [48]. Adapted from Advanced Materials journal with permission.

Ferromagnets are characterized by magnetization, which is mainly due to the alignment of localized electron spins and their associated magnetic moments in a specific direction in space, compared to non-ferromagnetic materials, which have a larger collective magnetic moment and Magnetization. The main way to change the direction of the magnetic moment is by applying a magnetic field. Significant discoveries in the fields of condensed matter and materials physics have emerged to enrich the available means of manipulating device magnetization, thereby accelerating the development of ferromagnetic memristors [49]. Saleem *et al.* used the electromagnetic field to control the material to realize the phase change and observed the magnetic transition. This huge change in the magnetic moment leads to the resistance-switching phenomenon of the device [50]. Sun *et al.* used the method of magnetron sputtering to

manufacture devices with magnetic switches and electric switches and realized a new spintronic device with resistance change at room temperature [51].

Ferroelectric Random Access Memory (FeRAM) is a commercial product that encodes information employing ferroelectric polarization and features a long read/write cycle life, low power consumption, and fast write speed. Its advantages of wide material selection and clear mechanism provide great advantages and application prospects and thus have been sufficiently studied [52]. In the study of In_2Se_3, synaptic plasticity and ultra-large resistance-to-switch ratio was achieved, and the polarization at each paired terminals of the device is the key to this property, and machine learning and high-precision image recognition were performed in neural networks [53]. Xue *et al.* explored the influencing factors of ferroelectric resistive switching and found that the degree of polarization, the degree of Schottky barrier change and the initial barrier height have an impact on device performance, and at the same time realized a ferroelectric volatile/non-conductive switch with a large on/off ratio [54].

However, the existence of some defects hinders the scalability of FeRAM. For example, the excessive thickness of the ferroelectric layers of the devices results in very low read currents, limiting their miniaturization [55]. When the thickness of the ferroelectric layer is reduced to a few nanometers, due to the quantum mechanical tunneling, electron conduction is greatly enhanced which is undesired [55]. Besides, since the capacitive readout of information requires ferroelectric polarization, it is a destructive readout that requires rewriting the information after readout [56].

1.4 Vacancy migration & Multi-state memristor

In memristors based on metal oxides, the conductive filaments theory cannot explain the principle. The resistance-switching behavior in the device is mainly due to the change in the Schottky barrier caused by the migration of oxygen vacancies. This barrier-based device has a special rectifying effect, which brings the possibility of realizing multi-resistance states. However, due to the rectification effect, the current in the device tends to be unstable. In addition, because of the higher barrier brought by the outer voltage, the device usually needs to operate at a high voltage, which is not preferable to reducing the power consumption of the

device [57]. Therefore, improvements in metal oxide memristors are needed. Agglomeration of oxygen vacancies has been observed in $LiNbO_3$ single-crystal, leading to on-off ratios on the order of 10^2 [58]. Wu *et al.* used the rectification effect and switching effect in the device to realize the dynamic pn junction, to fully suppress the current loss, and the device has great potential in high-density NRAM [59]. The injection and capture of carriers are achieved by controlling the depletion of the Schottky junction by the electric field. Lv *et al.* obtained a low-current, multi-state memristor in the experiment. The device has a good high-to-low resistance ratio and low device-to-device variation [60].

As a result of rectifying effects, multi-resistive memristors can be understood as devices that exhibit variable resistance values in response to specific inputs. This means it can be used as a logic encoding and multi-bit storage unit. To realize high-density memory, the ability to store multiple states in a single memristor cell is necessary. The advantages of high density and low power consumption make multi-resistive memory competitive with dynamic random access memories (DRAM) [61]. However, the adoption of multi-state memory in traditional von Neumann architectures results in a significant increase in power consumption, area, and more importantly, its processing inefficiency [61]. As a multi-bit memory unit, faster and more energy-efficient memristors can leverage computing-in-memory (CIM) to address this inefficiency, and neuromorphic and artificial neural network hardware is built [62-71].

Multi-resistive memristors have sufficient advantages in logic gate operations. Thanks to the multiple output results of the multi-state, operations of two or more logic gates can be realized on a single device. Ng *et al.* observed multi-resistive states on the prepared device and designed a three-value logic operation, successfully establishing an analog programming window [72]. In the study of true random number generators (TRNG), Nikolaos Vasileiadis used the random resistance property of multi-resistive memristors to increase the total entropy of the circuit [73]. In a neural network using a multi-resistive memristor architecture, the total power consumption of the array is reduced by more than 50% as the temperature increases without reducing the output power [75]. In summary, multi-resistive memristors with rectification effects are being explored in neural network simulation, logic programming operations, and new computer components. The advantages of low power consumption, high integration, and easy preparation

make multi-resistive memristors stand out among a variety of new electronic components.

1.5 ZnO memristor

In general, most memristors are built using a simple layer-layer structure consisting of electrodes and functional layers, typically in the form of vertical structure, parallel structure and cross-bar structure (Figure 1.5). Functional layers usually consist of dielectrics. The dielectrics used are mainly binary oxide materials such as nickel oxide (NiO) [76], copper oxide (CuO) [77], aluminum oxide (Al_2O_3) [78]and zinc oxide (ZnO) [79]. Memristors made from these materials show promising resistive switching properties. Resistive switching devices based on NiO dielectrics have been documented in many references [80]. It has a large on/off ratio and unipolar switching characteristics. However, there are many related issues that limit the development of NiO memristors. One of the most important issues is that such devices can require high reset currents, which makes them less suitable for low-power applications. For CuO-based memristors, one of its advantages is that CuO is compatible with CMOS processes, but CuO materials are not conducive to mass application due to their toxicity to the human body [81]. Al_2O_3 is another widely used dielectric material. It is usually used in low current applications, but this also limits the use of Al_2O_3 in high temperature and high current environments [82]. Compared to the limitations of appealing materials, ZnO has attracted much attention due to its wide bandgap, chemical stability, and high thermal conductivity [83]. Furthermore, zinc oxide is widely used because of its biocompatibility and biodegradability. This is why ZnO memristors not only have excellent working characteristics [84], but also can be applied in the fields of environment-friendly electronic devices and biodevices [85][86].

ZnO thin films have been produced by various techniques, mainly those requiring vacuum conditions, such as atomic layer deposition [87], pulsed laser deposition [88][89], and magnetron sputtering [90-93]. ZnO has also been extensively studied in terms of chemical pathways, such as electrochemical deposition [94] or sol-gel [95-98]. Compared with other deposition methods, magnetron sputtering has the characteristics of high repeatability, smooth deposited film, and good film adhesion [99].

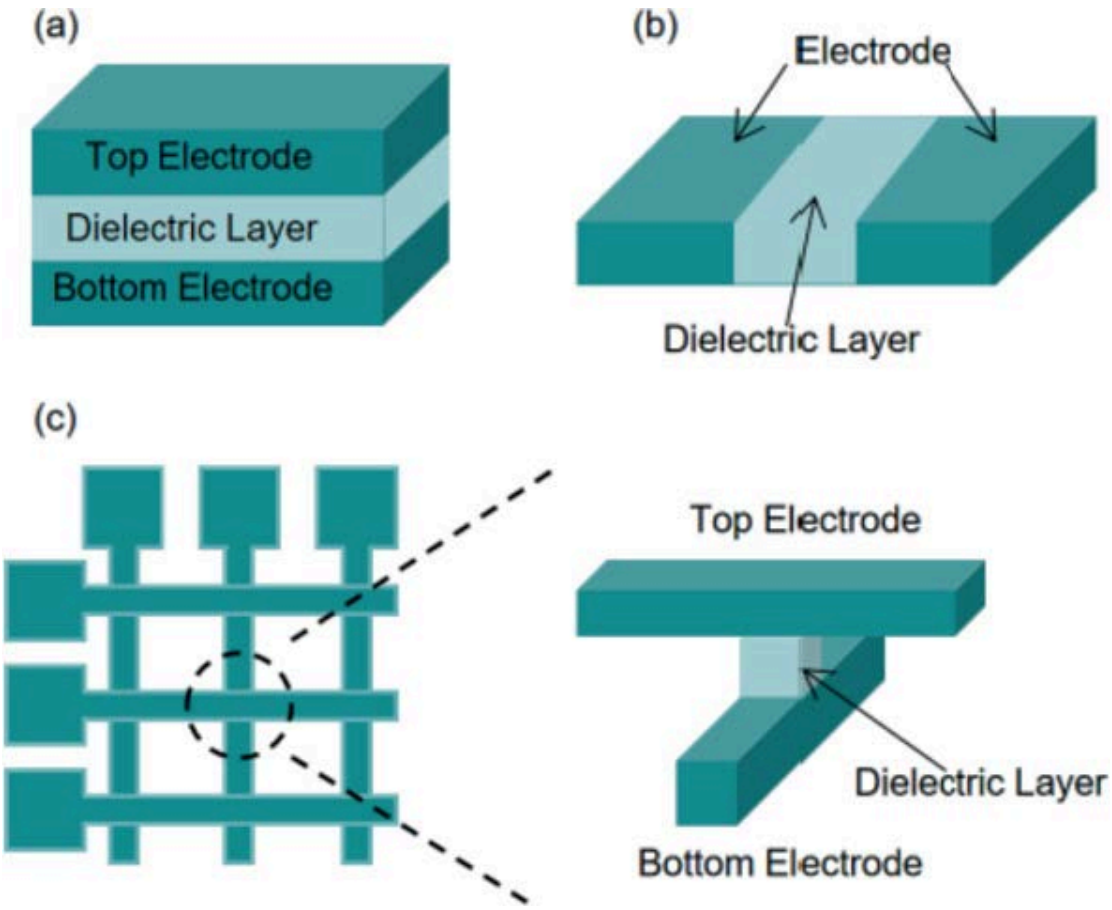


Figure 1.5 (a) Vertical structure. (b) Parallel structure. (c) Cross-bar structure [74]. Adapted from Interdisciplinary Research for Printing and Packaging with permission.

Although ZnO memristor has many advantages, its development still faces several challenges: the first is variation, in addition to device-device variation, there is also the degradation of device specificity with the working time, which is due to the fact that the device is not caused by defects that are completely consistent and cannot be recovered in a short time [100]. Secondly, the resistance switching mechanism of ZnO memristor still needs further research. As mentioned above, people have proposed different mechanisms for memristor, but because the experimental phenomena observed by different research teams are not completely consistent, so in different There is no consensus as to which mechanism is dominant in each case [101]. Finally, ZnO memristors still need to be improved due to their compatibility with complementary metal-oxide semiconductor (CMOS).

1.6 Phase change memory

Phase-change material (PCM)-based RAM (PRAM) is a commercialized memory technology. Array-based memory (Figure 1.6b) co-produced by Intel and Micron has entered the market as storage-class memory [102][103]. The device is slightly slower than high-performance dynamic random access memories (DRAM), but has a larger storage capacity and non-volatile capabilities. This PCM-based storage device product is an important step towards replacing solid state disk (SSD) and DRAM [104]. The advantage of PRAM lies in the read time and storage density, because PCM can achieve switching times of a few nanoseconds or even sub-nanoseconds in microscopic-sized memory cells [105], and the size can be further reduced [106]. In addition, the manufacturing cost of PRAM is also competitive, because the cost per GB of PRAM is about 10-100 times lower than that of common DRAM and static random access memories (SRAM) in the market (Figure 1.6a).

Figure 1.6c is a schematic diagram of the RS behavior of a phase change material. In phase change devices, the local temperature is achieved by applying Joule heating, which is usually controlled by voltage pulses or laser light of different frequencies and intensities. First, the reset process is to achieve amorphization by applying short and high pulse current or laser to the material, heating the material beyond the melting point and then cooling it rapidly. When the phase-change material is amorphized, the device is in a high-resistance state, which is usually defined as logic state 0. Then, a long and low pulse current or laser is applied to the material to achieve the SET process, in which the material is heated to the crystallization temperature, after which the material crystallizes to a low resistance, also defined as logic state 1 [108].

Through the above operations, the phase change memory can realize the RS behavior in a very short time and a large ratio of the high resistance state to the low resistance state. The phase transition between the two states is fast and reversible, and it also has good thermal stability at room temperature, both of which ensure the retention time and speed required for non-volatile phase transition applications. Therefore, the investigation of crystallization kinetics is a basic requirement to improve the performance of phase change memory [109-111].

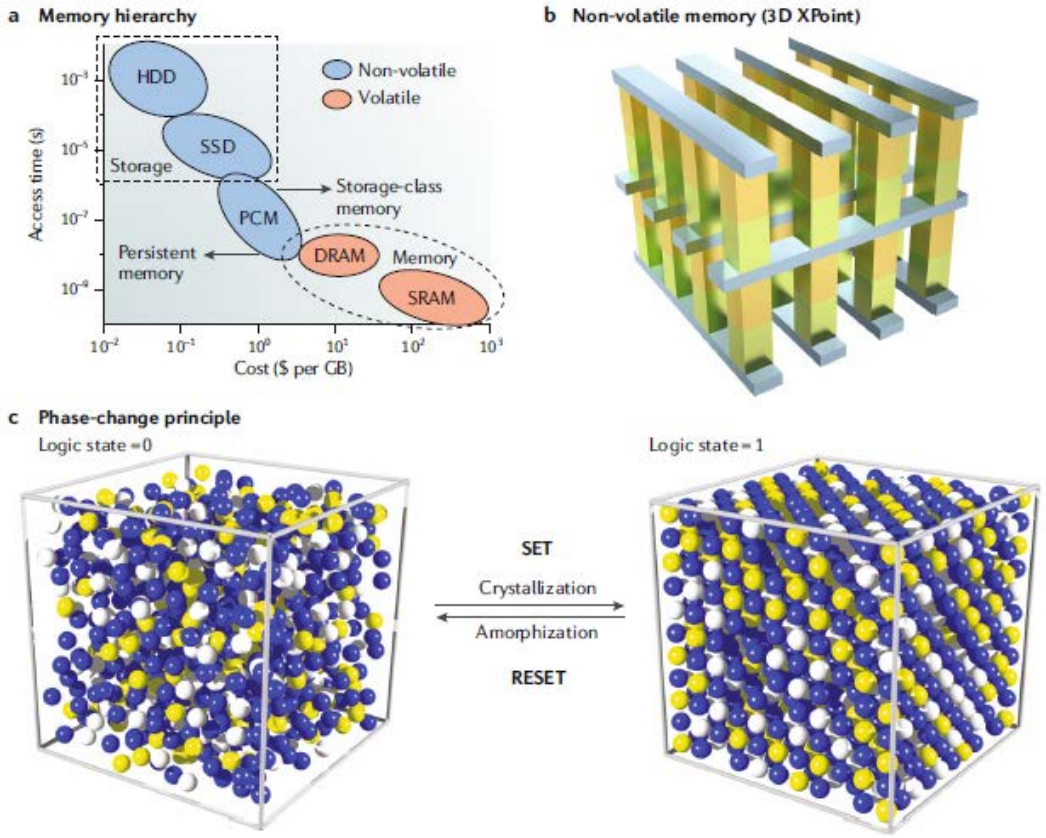


Figure 1.6 (a) Speed versus price per GB of various memory and storage [107]. (b) 3D Xpoint setup[102]. (c) Phase change principle [108]. Figure a. and Figure c. adapted from IEEE journal and Nature journal with permission, respectively.

Due to its special properties and promise in the market, phase change memory still has ample room for improvement in terms of materials, neural network applications, and crystallization kinetics. Joshi *et al.* prepared a superlattice-based phase change memory and optimized the scheme when performing convolutional neural network training and learning on the device to achieve ultra-high precision in long-term learning [112] Theoretically, Sun *et al.* explained the important role of excess germanium in the amorphous phase, and proposed a new phase change memory architecture with balanced speed and stability [113]. Meanwhile, phase-change material-based simulated memory synapses have the potential to generate precisely timed spikes in spiking neural networks (SNNs), which provides opportunities for combining signals generated by biomimetic sensors with neural network learning systems [136]. Thanks to its high integration, a wide range of modulation methods and high-speed resistive switching

behavior, phase-change memory has great potential in fields of next generation memory, high temperature electronic device and computer processing module. Further research on its mechanism and performance development is profound influence.

1.7 Sb_2Te_3 phase change material and its fabricating methods

Phase change materials are usually located in the Ge-Sb-Te (GST) ternary phase diagram (Figure 1.7) [114][115]. Besides the common GST, other materials in this phase diagram such as pure [116] or alloyed [117][118] Sb and doped Sb2Te3 [119] and Sb are also frequently investigated and have excellent electrical properties. As previously mentioned, exploiting the fast and reversible transition between amorphous and metastable crystalline phases of PCMs can enable applications for data storage, such as crystallization by Joule annealing or crystal formation by melt quenching. Both phases are very stable, lasting ten years under ambient conditions [120-122]. Such a rapid and stable transition of phase change materials has been attributed to some structural similarities between the two phases. GeTe-Sb_2Te_3 (GST) is the most widely studied phase change material due to its overall outstanding properties [123-126], where Sb_2Te_3 exhibits an extremely fast phase transition between its crystalline and amorphous state, thus attracted increasing interest [127][128]. However, the higher electrical conductivity of the crystalline state and the lower thermal stability of the amorphous state limit the practical application of Sb_2Te_3 in PCM devices [129][130].

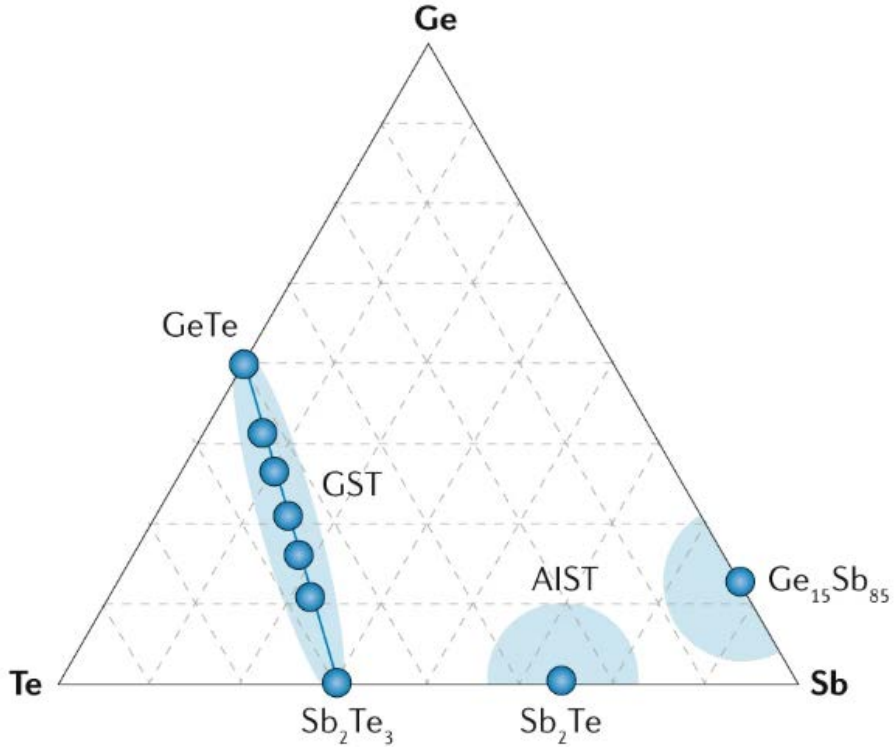


Figure 1.7 The important classes of phase-change materials (PCMs) are found in the Ge–Sb–Te ternary diagram [131]. Adapted from Nature journal with permission.

Since Sb is metal and Te is chalcogen, Sb_2Te_3 is a kind of chalcogenide metal material, which is widely prepared via chemical vapor deposition (CVD) method. As a typical bottom-up method, CVD offers a compromise between controllability, high efficiency, scalability and high quality. More importantly, the CVD method has shown outstanding advantages in synthesizing 2D materials at the atomic level, which is conducive to comprehensive understanding the relationship between material structure and properties [132].

Chemical vapor transport (CVT) method represents a kind of reactions with one common feature: the sublimation of a condensed phase in the presence of gaseous reactants, which is then deposited as crystalline [133]. Notably, CVT differs from CVD, the main difference between them is the state of the precursor, with CVD typically using gaseous precursors and CVT typically using solid reactants. This leads to differences in reactor design and product characteristics. Since the CVT method discovered in 1851, people have a comprehensive understanding of the CVT in terms of experimental exploration and theoretical modeling [134]. Furthermore, CVT has been employed and produced a wide variety of crystalline solids,

including metals, intermetallic phases, metal oxides, halides, chalcogenides, and chalcogenide halides [134][135]. Knowledge about the CVT method and extensive experimental experience can provide opportunities for the controlled synthesis of 2D materials and the exploration of novel 2D materials. Unfortunately, in stark contrast to the wide application of CVD in the preparation of 2D materials, the CVT method has not attracted enough research interest.

1.8 Summary

Electronic devices with resistive switching behavior offer several advantages over existing processors in terms of power consumption, area, speed, and functionality. However, there are still various challenges in the preparation of materials, working life, stability, etc. In this thesis, a ZnO memristor with multi-state, low device-device variation and long-term stability is successfully realized, its LTP and LTD tests are carried out to verify the possibility of its application in neuromorphic computing. Schottky emission theory explained its resistive switching mechanism, and finally simulated a logic operation coupled with an AND and OR by using the multi-resistance state of the device. In addition, this article will discuss the scheme and feasibility of preparing crystals consist of Sb and Te in two different methods: CVD and CVT, as a possible phase change materials for memristors.

2. Asymmetric-resistive-switching device with reconfigurable synaptic functions for logic operations

2.1 Overview

Memristors can be used in neural network computing. In this chapter, Mo/ZnO/ITO (in the order of bottom to top of device) memristors are prepared. Resistive switching behavior with rectification effect and reliable stability are observed. LTP and LTD tests were carried out on the device, the resistance-switching mechanism was demonstrated by using the Schottky emission theory. A coupling logic operation scheme is designed.

2.2 Experiments and Methods

2.2.1 Device fabrication

The wafer with thermal wet oxide SiO_2 (300 nm) was used as the substrate. The device was fabricated in order of Mo, ZnO and ITO (Indium tin oxide) (from the bottom to the top). At first, the substrate was ultrasonically cleaned in acetone, IPA and water. The electrode (ITO and Mo) and active layer (ZnO) were deposited by AJA magnetron sputtering with a background pressure of $5x10^{-7}$ Torr. Mo metal was used as a bottom electrode which was deposited by direct current (DC) magnetron sputtering with the target Mo. The sputtering power was 100 W, the deposition pressure was 5 mTorr and the working gas was pure Ar. Radiofrequency (RF) magnetron sputtering was used to deposit ZnO. The source target was ZnO, the sputtering power was 200 W and the deposition pressure was 5 mTorr. The gas flow of Ar/O_2 was 24 sccm/1 sccm. Then the shadow mask was utilized to fabricate the device, which has the same size as mask of 100 um. The ITO was deposited by RF magnetron sputtering. The target was ITO, the deposition power was 100 W, the deposition pressure was 5 mTorr and the working gas flow of Ar/O_2 was 20/0.3. The deposition temperature of ITO was raised to 200 ℃ (substrate temperature).

2.2.2 Material and device characterizations

Scanning Electron Microscopy (SEM, Hitachi SU5000 FESEM) images were captured, whose

accelerating voltage was 12.5 kV. The Energy Dispersive X-ray Spectroscopy (EDS, Hitachi SU5000 FESEM) was used for materials composition mapping. Grazing Incidence X-ray Diffraction (GIXRD, PANalytical X'Pert PRO system) was utilized to study the crystal structures of materials. X-ray photoelectron spectroscopy (XPS, Thermo-VG Scientific ESCALab 250) was employed to investigate the surface characteristics of materials. Ultraviolet photoelectron spectroscopy (UPS, Thermo-VG Scientific ESCALab 250) was used to measure the work function (Φ) of material surfaces. The electronic properties were analyzed by a Keysight B2985A source meter with the probe station.

2.3 Results and Discussion

2.3.1 Material characterizations

The asymmetric RS device was fabricated in the order of Si/SiO_2/Mo/ZnO/ITO (bottom to top). As shown in Figure 2.1a, the ZnO film is relatively smooth and crack-free, and the ratio of Zn and O is close to 1:1. As shown in Figure 2.1b, the surface of ITO is dense and crack-free. From EDS result in Figure 2.1b, In, Sn and O in the ITO electrode are uniformly distributed, and the O content in ITO is higher than that of In and Sn, which is important for the generation and migration of oxygen vacancy [137]. The crystal structure of the film was further investigated using grazing incidence X-ray diffraction (GIXRD), as shown in Figure 2.1c. The strong peak at 34.3° is attributed to the (101) plane of ZnO, which can also find characteristic peaks corresponding to ZnO (102) and ZnO (103) at 47.4° and 62.7° [138], the results confirmed that no impurity phase, only characteristic peaks of the desired material were observed. In addition, X-ray photoelectron spectroscopy (XPS) was employed to deeply study the chemical state of the material surface. In the XPS spectrum of ZnO, two peaks with binding energies at 530.3 eV and 532.3 eV were observed in the O 1s spectrum (Figure 2.1d), corresponding to O2- and absorbed oxygen in Zn-O bonding. In the Zn 2p spectrum, two characteristic peaks at 1044.6 eV and 1021.4 eV were observed, corresponding to Zn 2p1/2 and Zn 2p3/2, respectively. The splitting of these spin-orbit components is around 23.2 eV, which confirms the +2 state of the Zn atom [139]. In addition, the work function (Figure 2.1f) of the active layer was measured to study the energy band relationship in the device, which is calculated to 4.64 eV. Materials

characterization indicated that high-quality materials were prepared concerning surface morphology, composition distribution, and crystal purity. This is crucial for high-performance multi-state memristor devices.

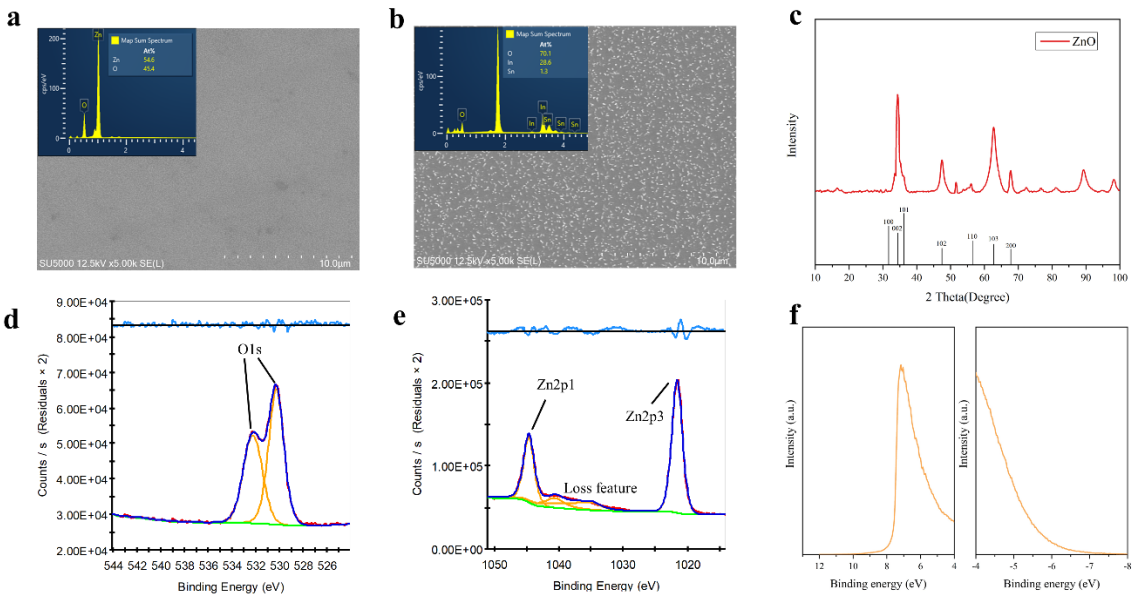


Figure 2.1 (a) The SEM image & EDS results of ZnO. (b) The SEM image & EDS results of ITO. (c) XRD result of ZnO. (d) & (e) XPS result of ZnO. (f) UPS result of ZnO.

2.3.2 Electronic performance

When performing electronic test on the device, the ITO (top) electrode was connected to positive voltage and the Mo (bot) electrode was conducted to negative voltage. The electronic synapse performance including memristive effect and LTP & LTD were studied. The I-V curves of ARS (asymmetric-resistive-switching) and its long-term stability were shown in Figure 2.2a. The loop has the characteristic shape of a hysteresis loop. This indicates the typical memristive effect [140]. The device was originally at a high resistance state (HRS), when the positive voltage was applied, the device switched to a low resistance state (LRS), which would have a higher current at the same voltage compared to the device at HRS. Reversely, once the negative voltage was applied the device was switched from LRS to HRS since the current was lower at the same voltage. The long-term stability was tested with the same parameters for 100 cycles and the device represented excellent stability and no degradation since the curve maintained its tendency after 100 cycles. Notably, the resistance switching was asymmetric, which is also

called the rectification effect, that comes from the change of Schottky barrier height, which benefits the multi-state of the device and contributes to neuromorphic computing. As shown in Figure 2.2b, ARS provided 4 different conductance, which means the multi-state of the device is more than the general memristor with only LRS and HRS. The device was test at 0.2 V for 3000 S. The device has 4 stable states with small variation, whose average conductance are 42.29 nS at LRS under positive voltage, 25.93 nS at LRS under negative voltage, 17.18 nS at HRS under positive voltage and 4.25 nS at HRS under negative voltage, respectively. The device-to-device variation is important for synaptic simulation and neuromorphic computing [141]. To apply the device in neuromorphic computing, LTP and LTD were obtained (Figures 2.2c & 2.2d). In Figure 2.2c, the synaptic plasticity does not fluctuate after 10,000 tests, and there is a clear difference between nerve impulses (red and bule lines) when positive/negative voltage pulse were applied. This further shows that the device has good stability and remarkable output results in neural computing. Zoom in Figure 2.2c to obtain Figure 2.2d, more details were observed. The results of LTP and LTD tend to be straight lines, which indicates that the devices can simulate nerve impulses very well [119]. Besides, the results of each pulse are similar, which proves that the device can output stable results when performing neural computing. The synaptic plasticity tests show that the memristors can be perfectly incorporated in neural computing.

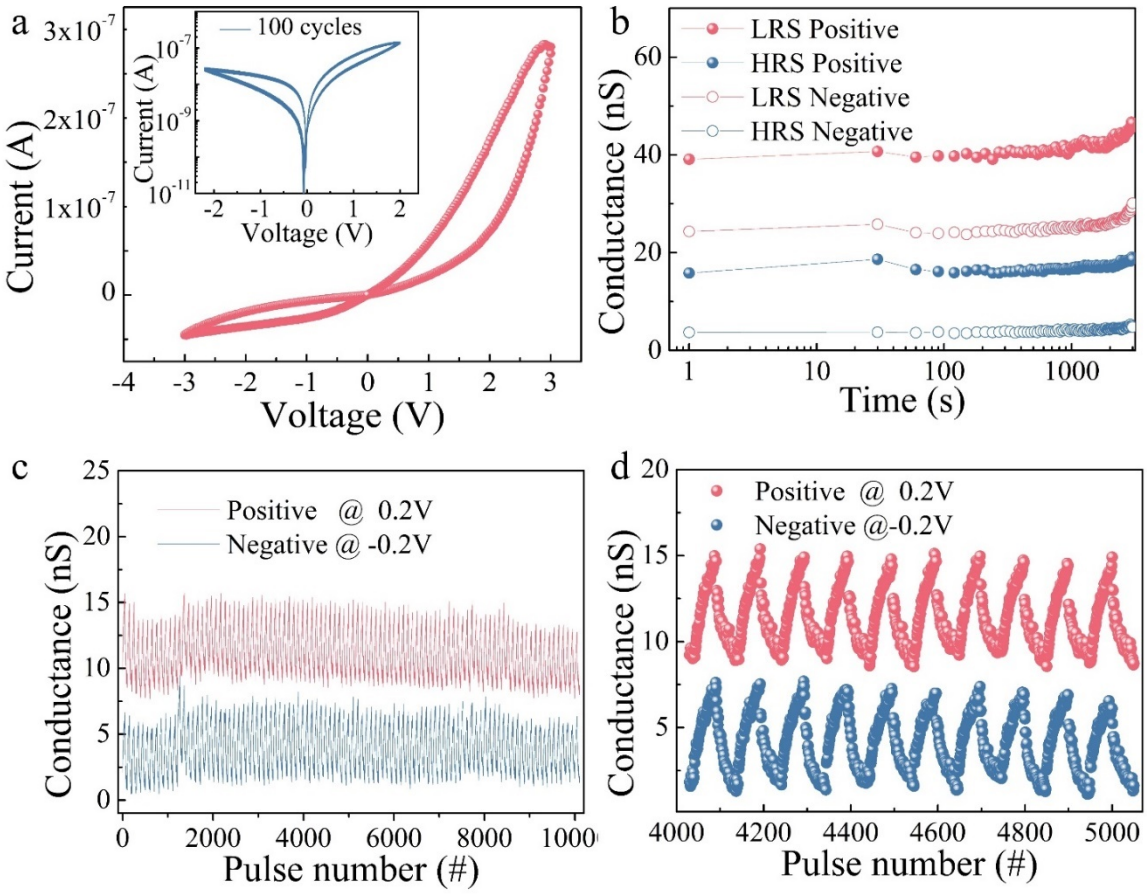


Figure 2.2 (a) I-V curves of the device with ARS, in which the red curve shows the asymmetric Reset/Set process and the blue curve indicates long-term stability. (b) Conductance of device at HRS/LRS under positive/negative of the same amplitude voltage. (c) and (d) Potentiation/depression properties of the device under positive/negative electronic pulses, whose duration was 100 ms.

2.3.3 The mechanism of ARS

The mechanism of ARS was studied from both Schottky emission theory and experimental measurements. Considering oxygen vacancies as a factor that induces ARS. According to Schottky emission theory, the emission would happen once the electrons gain energy to overcome the energy barrier [143]. As a result of emission, the switching behavior is realized by modulating the barrier height, which is accomplished by varying work function via injecting oxygen vacancies into ZnO. The Schottky emission (Thermionic emission) is described by the Richardson equation [143]:

$$J = A_G T^2 e^{\frac{-(W-\Delta W)}{kT}} \qquad (1)$$

Where AG is the Richardson constant, T is the temperature of the device, W means local work-function, ΔW presents the amount of the electric field lowers the surface barrier, k means Boltzmann's constant. To describe AG, W and ΔW, the equations are utilized:

$$A_G = \frac{4\pi q m^* k^2}{h^3} \qquad (2)$$

Where m* is the effective mass of electrons, h is Planck's constant,

$$W = q\emptyset_B \qquad (3)$$

Where ∅B means the barrier height,

$$\Delta W = \sqrt{\frac{q^3 E}{4\pi\epsilon_0}} \qquad (4)$$

Where E represents the electric field and ε0 is the electric constant. Equation (1) can be transformed into:

$$\ln(J) = \frac{q}{kT}\sqrt{\frac{q}{4\pi\epsilon_0}} \times E^{\frac{1}{2}} - (\ln\frac{h^3}{4\pi q m^*(kT)^2} + \frac{q\emptyset_B}{kT}) \qquad (5)$$

According to Equation (5), ln (I) and $E^{1/2}$ have a linear relationship. In Figure 2.3a, ln (I) of the device at HRS increased linearly as $E^{1/2}$ elevated, following the temperature rising for 10 degrees per time, the curves sustain linear without prominent change on slopes of fitting lines, which represents that Schottky thermionic emission dominated the ASR mechanism. Equation (5) can be converted to:

$$Ln\left(\frac{I}{T^2}\right) = Ln\left(\frac{4\pi S q m^* k^2}{h^3}\right) - \frac{q(\emptyset_B - \sqrt{\frac{qE}{4\pi\varepsilon}})}{k} \times \frac{1}{T} \qquad (6)$$

With a constant electric field intensity E, $Ln(I/T^2)$, and 1/T should have a linear relationship. In Figure 2.3b, the plot of $Ln(I/T^2)$ vs. 1000/T for the device at HRS showed a linear relationship which was coincident with Equation (6). Figure 2.3c displays the schematic diagram of the energy band for the device at HRS. Once the device switched into LRS, since the barrier height was reduced, there occurred a part of Ohm contact which caused the fitting line to follow the relationship of log(|I|) vs. log(|V|) as shown in Figures 2.3d and 2.3e, when the device was under

positive and negative voltage, respectively. In the context of semiconductors and insulators, an increase in the number of vacancies generally leads to a decrease in the barrier height. The reason is as follows: vacancies can introduce local energy levels within the bandgap. The introduction of energy levels through vacancies can affect the position of the Fermi level. If the energy levels introduced are closer to the conduction band, they can act as donors, increasing the concentration of electrons in the conduction band and causing a lower barrier height for electrons to move through the material [144]. Figure 2.3f displays the schematic diagram of the energy band for the device at LRS. When a positive voltage is applied across the device, oxygen vacancies are located at the ZnO/ITO interface, and the Schottky barrier height decreases due to the increased concentration of oxygen vacancies, which leads to a decrease in device resistance. Switch the device from HRS to LRS by applying a positive voltage (SET operation). Accordingly, a negative voltage is applied across the device to remove oxygen vacancies and restore the original barrier height, thereby switching back to HRS (RESET operation). Notably, the barrier height and ZnO conductivity gradually changed with the migration of oxygen vacancies, which indicates that the conductivity of this device can be modulated, it is crucial for simulating synapses.

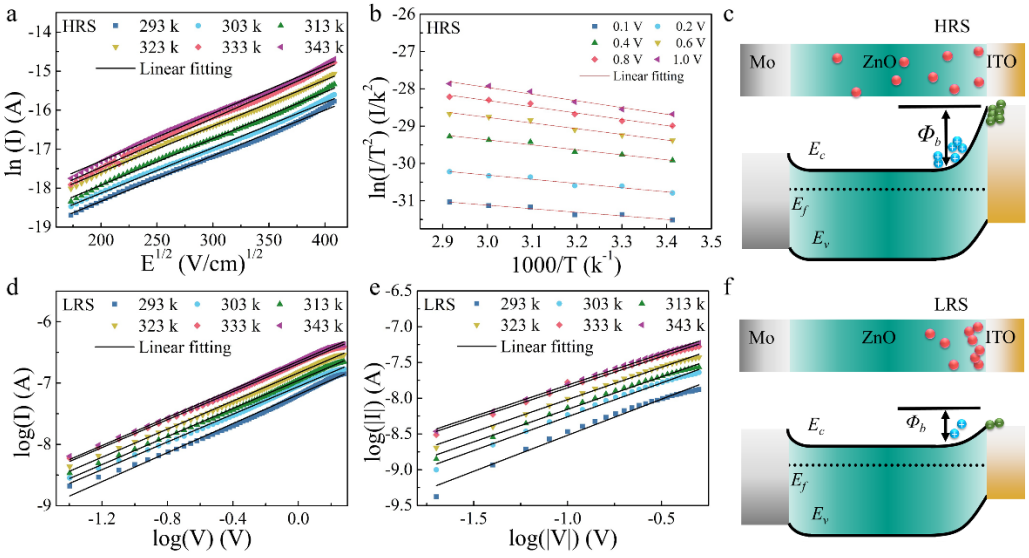


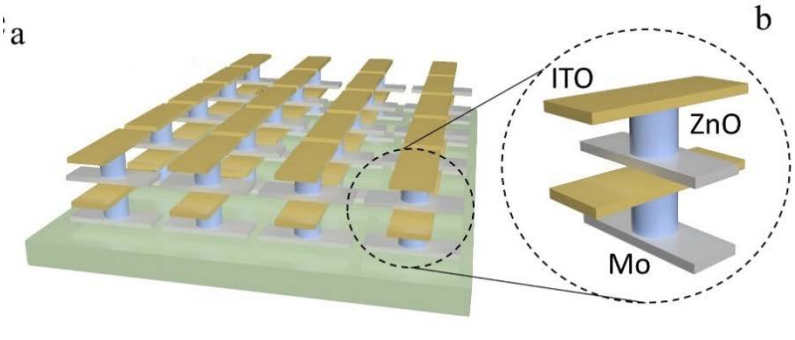
Figure 2.3 (a) The fitting line of ln(I) vs. E1/2 for the device at HRS. (b) The fitting line of ln(I/T2) vs. 1000/T for the device at HRS. (c) Schematic diagram of energy band for the device at HRS. (d) The fitting line of log(I) vs. log(V) for the device at LRS under positive voltage. (e)

The fitting of log(|I|) vs. log(|V|) for the device at LRS under negative voltage. (f) Schematic diagram of energy band for the device at LRS.

2.3.4 Demonstration of logic operation based on multi-state memristor

In the basic computer logic language, "0" and "1" as the simplest binary units can realize various functions through complex logic composition. How to use the multi-resistance advantages of memristors to complete logic expression on hardware without the support of software systems is very worthwhile. RS devices can be applied to information storage and logic operations if HRS is defined as logic “0” and LRS as logic “1” [145]. From Figure 2.2b, the four conductance of the device are 42.29 nS and 17.18 nS under the positive voltage, and 25.93 nS and 4.25 nS under the negative voltage, which means that the device has 4 states under the control of the outer source. Compared with regular memristors, the device has more resistance states so that more kinds of logic gates can be coupled. Since the HRS and LRS of the device are not equal to the conductance when the positive/negative voltage is applied, when two devices (device 1 & device 2) are connected in series as a unit and the positive/negative voltage is applied (Figure 2.4a), the conductance of every unit would be the sum of two individual ARS memristors, based on their 4 conductance, 6 different conductance of single unit gained: 84.58 nS, 59.47 nS and 34.36 nS at a positive voltage, 51.86 nS, 30.18 nS and 8.5 nS at a negative voltage. The switching of the potential difference in the circuit can be realized simply by two switches. Since the "0" signal can be regarded as background noise in the process of signal transmission and recognition, here the output signals 34.36 nS and 8.5 nS are not discussed in Figures 2.4c & 2.4d when the input signal is in a high-resistance state. Set the threshold to 40 nS, the signal output above the threshold is “1” and the output is “0” when the signal is below the threshold. The disparate conductance provides different output signals for logic operations under voltages with different directions. Figures 2.4c & 2.4d demonstrate the logic operations of AND and OR, which correspond to the truth table as shown in Figure 2.4b, which shows that OR/AND logic is executable. Conspicuously, as a result of voltage modulating and its advance of multistate, the device realizes the multi-functional logic operation of the AND gate and the OR gate without a software system. Compared with similar devices, the device has the advantages of

multi-function, reliable hardware and simple structure [145]. The device demonstrates the advances of economics and integration, in addition, it also provides a wider application field and more new paths for the research and development of memristors.



b

Input		Output	
Device 1	Device 2	OR	AND
0	0	0	0
1	0	1	0
0	1	1	0
1	1	1	1

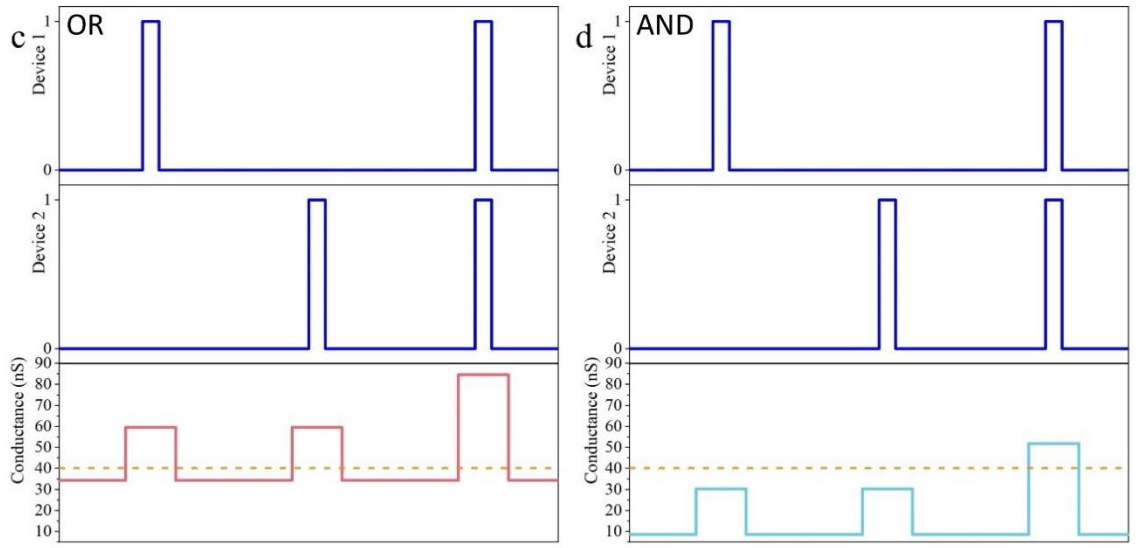


Figure 2.4 (a) Schematic diagram of the device applied in logic computing. (b) AND & OR logic truth table. (c) A demonstration of OR logical operation. (d) A demonstration of AND logical operation. The dotted line in Figure 2.4 c & d is the threshold 40 nS.

2.4 Summary

In this work, an electrically regulated asymmetric-resistive-switching memristor with coupled logic gate operations has been fabricated to advance the application of neural computing. The device is a two-terminal device based on the widely used metal oxide ZnO, which is compatible with the general magnetron sputtering process. ARS memristors enable long-duration and stable simulation of nerve impulses with 4 distinct resistance states. It provides an idea for a single device to realize multiple logic gate operations under electrical modulation.

Simultaneously, a stable resistive switch under electronic stimulation was observed. Schottky emission was used to explain the resistive switching mechanism, the barrier height can be modulated by controlling the migration of oxygen vacancies to affect the conductance of ZnO. This electrically regulated ASR multistate memristor can be used in neuromorphic computing and complex logic gate operations.

3. Sb_2Te_3 phase change crystal material preparation

3.1 Overview

The excellent properties of phase change materials are very dependent on the preparation conditions. In this chapter, the CVD method and CVT method are used to prepare Sb_2Te_3 crystal material. Micro-crystals on the substrate and crystals with a diameter of 1.5 cm were obtained respectively. Material characterization was performed.

3.2 Experiment and Methods

3.2.1 Chemical vapor deposition (CVD) method

A wafer with hot wet oxide SiO_2 (300 nm) was used as the substrate. Crystals are deposited on silicon wafers by the CVD method in a tube furnace. First, the substrate is ultrasonically cleaned in acetone, IPA, and water. Weigh 200 mg of Sb powder and 300 mg of Te powder then place them in two quartz boats, respectively. The Te powder is placed upstream of the furnace (first temperature zone), the Sb powder is placed downstream of the furnace (second temperature zone). Place the substrate bot-side up on a quartz boat that holds Sb powder. The tube furnace was evacuated to a low vacuum, filled with argon, this step was repeated three times to remove impurities. During the reaction, the argon flow rate was maintained at 150 sccm. Raise the temperature of the second temperature zone from room temperature to 660°C, the heating time is 64mins, the temperature is kept for 10hrs. Maintain the temperature in the first temperature zone at room temperature for 18 minutes and then heat to 480°C for 46 minutes and keep the temperature for 10 hours. To achieve the purpose of 10hrs react time.

3.2.2 Chemical vapor transport (CVT) method

Encapsulate the material using an ampoule tube. Weigh 2 g of Sb powder and 3 g of Te powder then mix them uniformly, pour them into an ampoule tube. Place the ampoule tube in the tube furnace, adjust the position of the ampoule tube and temperature setting, to realize the

temperature gradient between the two ends of the ampoule tube which is from 650°C to 550°C. Use a vacuum pump to evacuate the tube below 10^{-2} torr. The reaction was running for 4 days.

3.2.3 Material characterization

Scanning electron microscope (SEM, Hitachi SU5000 FESEM) images were taken with an accelerating voltage of 20 kV. Energy-dispersive X-ray spectroscopy (EDS, Hitachi SU5000 FESEM) was used for material composition mapping. X-ray diffraction (XRD, PANalytical X'Pert PRO system) is used to study the crystal structure of the material. Raman spectroscopy (Bruker Senterra-2 Raman) was used to study the degree of crystallinity of the material.

3.3 Results and Discussion

3.3.1 Material characterization for Sb_2Te_3 deposited on wafer

As shown in Figure 3.1a-d, many tiny hexagonal crystals are deposited on the SiO_2 substrate, the size difference of these hexagonal crystals is not significant. The crystals are evenly distributed on the substrate. This is consistent with the crystal structure of Sb_2Te_3 mentioned in the literature [146]. According to the EDS results (Figure3.1e-h), the elements are Sb and Te. However, the atomic ratio of Sb: Te in the mapping result is 65:35, which may be caused by the incomplete reaction of the material. In addition, the crystal size is about 3 ums, which indicates that the growth of Sb_2Te_3 by CVD is slow and highly volatile.

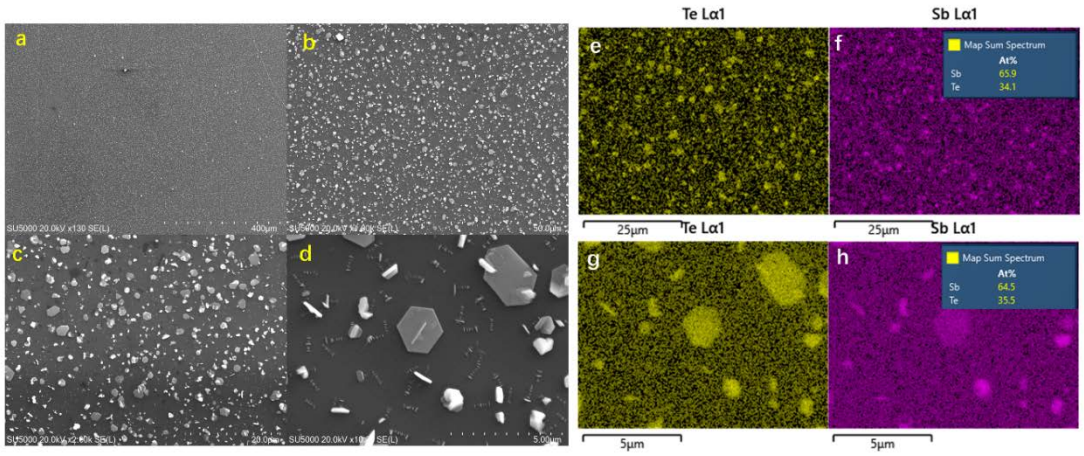


Figure 3.1 (a-d) The SEM image of the Sb_2Te_3 deposit on the wafer. (e-h) The EDS results and composition mapping of Sb_2Te_3

3.3.2 Material characterization for Sb_2Te_3 prepared by CVT

CVT, as a kind of fabrication to generate large quantities of phase change metals, is used here to prepare Sb_2Te_3 ingots. As shown in Figure 3.2a, a blocky crystal with metallic luster is formed in the ammeter tube, its diameter is about 1.5 cm, the toughness is good but the strength is low, so it can be mechanically exfoliated to obtain two-dimensional material. The SEM image shows that the crystal surface is uneven, which indicates that the crystal growth is not uniform and the material reaction is not complete. From the mapping of EDS, it can be seen that the distribution of material elements is affected by the flatness of the material surface. The results show that the atomic ratio of Sb and Te is close to 1:1. The results of SEM and EDS indicated that the crystal growth was too fast leading to its inhomogeneous formation, which was usually determined by the reaction time and temperature gradient.

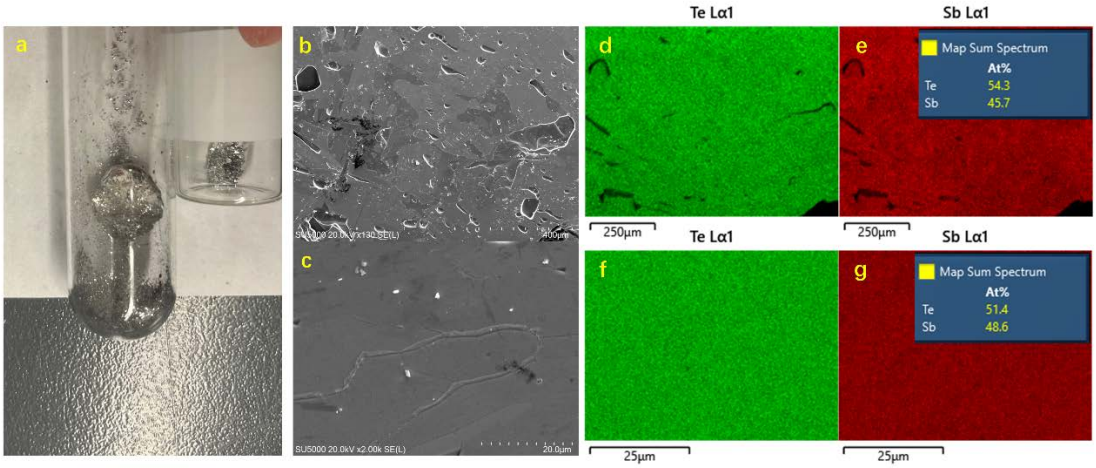


Figure 3.2 (a) The image of Sb_2Te_3 crystal prepared in the ampoule tube. (b) & (c) The SEM image of Sb_2Te_3 crystal. (d-g) EDS results and composition mapping of Sb_2Te_3 crystal

XRD and Raman spectra were tested on Sb_2Te_3 crystals. Comparing the XRD results with the standard card, it is confirmed that the crystal composition is $Sb_{0.4}Te_{0.6}$ (Sb_2Te_3) and Te simple substance (Figure 3.3a). This proves that the material reaction is not complete during the preparation process, which may be due to the higher melting point of Te, which leads to the slower evaporation and sublimation rate of Te in the reaction than that of Sb, resulting in the residue of Te that did not participate in the reaction. In the Raman spectroscopy test, a 785nm, 25mW laser is irradiated on the sample for 25s. The highest peak at 1350 cm^{-1} and the peak at 2700 cm^{-1} show that the crystal contains many defects, and its characteristic peaks are consistent with previous reports [147]. This proves that Sb_2Te_3 crystals were successfully prepared by CVT.

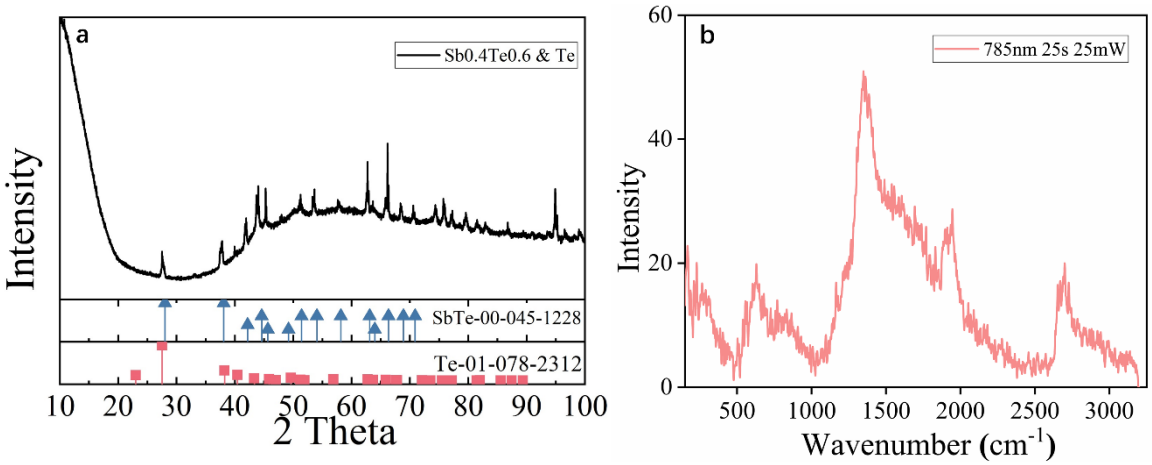


Figure 3.3 (a) XRD result of Sb_2Te_3 crystal. (b) Raman spectra of Sb_2Te_3 crystal

As mentioned above, the brittleness of the as-prepared Sb_2Te_3 crystals endows them with the possibility of mechanical exfoliation. Use Scotch tape to exfoliate the bulk sample and transfer it to the substrate. As shown in Figure 3.4 a & b, the layered crystal plate with a size of 20um was obtained. Directly observing the tape used for striping, there were layer crystals with a size of 500um, which shows that the material can be exfoliated well, but it is limited by factors in the transfer process such as mechanical viscosity, temperature, substrate material, etc. As a result of it, the size of the transferred crystals is reduced.

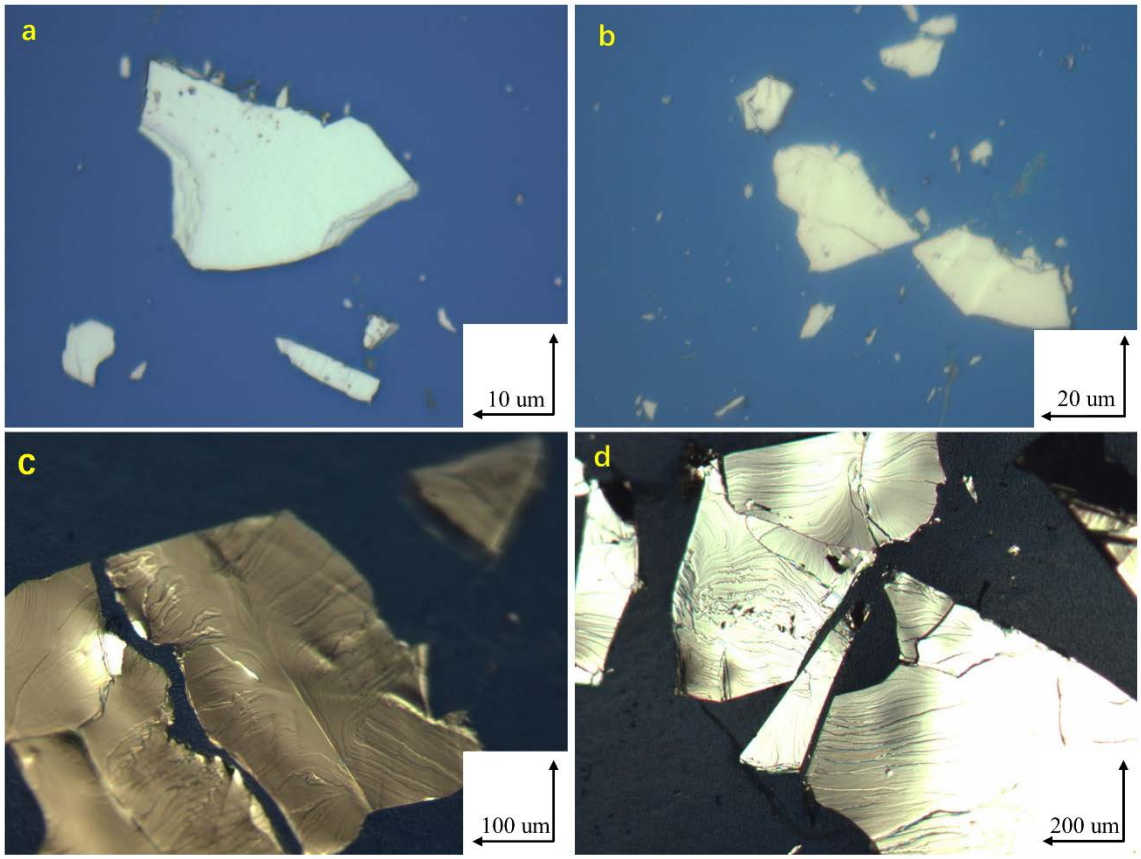


Figure 3.4 (a) & (b) Mechanical exfoliate crystal onto the wafer. (c) & (d) Mechanical exfoliate crystal onto the tape

3.4 Summary

The hexagonal crystal consists of Sb and Te is deposited on wafer by CVD method, and the Sb_2Te_3 crystals were prepared by CVT method CVD. The material was characterized by SEM, EDS, XRD, and Raman spectroscopy, which proved the successful preparation of the material.

4. Conclusion and future work

The research focuses on electronic devices with resistive switching behavior. Two RS devices based on different mechanisms were explored.

The first device with ZnO as the functional layer exhibits memristive behavior with rectifying effect. It is verified that the device can perform neural network computing. The mechanism is explained by Schottky emission theory. Its unique multi-state was used to design the coupling logic operation scheme.

In addition, the possibility of preparing Sb_2Te_3 phase change materials by CVD and CVT is discussed. The correctness of material preparation was confirmed. The optimization of the synthesis procedure will be explored in the future. The phase change memristor based on Sb_2Te_3 will be investigated in the future.

These new electrical devices have the advantages of high integration, multi-function, low power consumption, thermal stability, low device-to-device variation and long timeliness, they have promising prospects in the fields of artificial intelligence, machine learning and neuromorphic computing. This study promoted the research on the resistance switching mechanism of memristors, broadened the idea of device optimization, and contributed to the improvement of RS devices.

References

[1] G. Zhou, J. Wu, L. Wang, B. Sun, Z. Ren, C. Xu, Y. Yao, L. Liao, G. Wang, S. Zheng, P. Mazumder, S. Duan & Q. Song, Evolution map of the memristor: from pure capacitive state to resistive switching state. Nanoscale, 11 (2019) 17222–17229. https://doi.org/10.1039/C9NR05550A

[2] B. Sun, T. Guo, G. Zhou, J. Wu, Y. Chen, Y. Zhou, & Y. Wu, A Battery-Like Self-Selecting Biomemristor from Earth-Abundant Natural Biomaterials. ACS Applied Bio Materials, 4 (2021) 1976–1985.

[3] H. Wang, C. Gao, & X Yan, High-Performance and Multifunctional Devices-Based Optoelectronic Memory With the 2D Narrow Bandgap Bi2Te2.7Se0.3. IEEE Electron Device Letters, 41 (2020) 1504–1507. https://doi.org/10.1109/LED.2020.3017166

[4] S. Djokic, R. Langella, J. Meyer, R. Stiegler, A. Testa, & Xu. Xiao, On Evaluation of Power Electronic Devices' Efficiency for Nonsinusoidal Voltage Supply and Different Operating Powers. IEEE Transactions on Instrumentation and Measurement, 66 (2017) 2216–2224. https://doi.org/10.1109/TIM.2017.2706438

[5] R. Alishah, S. Hosseini, E. Babaei, & M. Sabahi, A new single-phase multilevel converter topology with reduced power electronic devices, voltage rating on switches, and power losses. International Journal of Circuit Theory and Applications, 46 (2018) 1372–1391. https://doi.org/10.1002/cta.2484

[6] Guo Z, Ma Y, Dong X, Huang J, Wang Y, Xia Y. An Environmentally Friendly and Flexible Aqueous Zinc Battery Using an Organic Cathode. Angewandte Chemie (International ed). 2018;57(36):11737-11741. doi:10.1002/anie.201807121

[7] Jaiswal, A.; Chakraborty, I.; Agrawal, A.; Roy, K. 8T SRAM Cell as a Multibit Dot-Product Engine for Beyond Von Neumann Computing. IEEE Trans. VLSI Syst. 2019, 27, 2556–2567.

[8] Iida, M.; Koga, M.; Inoue, K.; Amagasaki, M.; Ichida, Y.; Saji, M.; Iida, J.; Sueyoshi, T. A Genuine Power-Gatable Reconfigurable Logic Chip with FeRAM Cells. IEICE Trans. Electron. 2011, E94C, 548–556.

[9] Park, J.; Lee, M.; Kim, S.; Ju, M.; Hong, J. MH Cache: A Multi-Retention STT-RAM-based Low-Power Last-Level Cache for Mobile Hardware Rendering Systems. ACM Trans. Archit. Code Optim. 2019, 16, 1–26.

[10] Chiu, C.H.; Huang, C.W.; Hsieh, Y.H.; Chen, J.Y.; Chang, C.F.; Chu, Y.H.; Wu, W.W. In-situ TEM Observation of Multilevel Storage Behavior in Low Power FeRAM Device. Nano Energy 2017, 34, 103–110.

[11] Shadmana, A.; Zhu, J.G. High-Speed STT MRAM Incorporating Antiferromagnetic Layer. Appl. Phys. Lett. 2019, 114, 022403.

[12] Rzeszut, P.; Skowronski, W.; Zietek, S.; Wrona, J.; Stobiecki, T. Multi-bit MRAM Storage Cells Utilizing Serially Connected Perpendicular Magnetic Tunnel Junctions. J. Appl. Phys. 2019, 125, 025704.

[13] Lee, J.H.; Lim, D.H.; Jeong, H.; Ma, H.M.; Shi, L.P. Exploring Cycle-to-Cycle and Device-to-Device Variation Tolerance in MLC Storage-based Neural Network Training. IEEE Trans. Electron Devices 2019, 66, 2172–2178.

[14] Senni, S.; Torres, L.; Sassatelli, G.; Gamatie, A. Non-volatile Processor based on MRAM for Ultra-Low-Power IoT Devices. ACM J. Emerg. Technol. Comput. Syst. 2017, 13, 1–17.

[15] Elliott, S.R. Chalcogenide Phase-Change Materials: Past and Future. Int. J. Appl. Glas. Sci. 2015, 6, 15–18.

[16] Hwang, I.; Cho, Y.J.; Lee, M.J.; Jo, M.H. The Role of Contact Resistance in GeTe and Ge2Sb2Te5 Nanowire Phase Change Memory Reset Switching Current. Appl. Phys. Lett. 2019, 106, 193106.

[17] Lin, C.C.; Liou, H.Y.; Hung, P.H.; Chu, S.Y.; Huang, C.Y.; Hong, C.S. Effects of Film Orientation on Power Consumption, Thermal Stability, and Reliability of Aluminum Nitride Resistive Random Access Memory Devices. IEEE Trans. Electron Devices 2019, 66, 4716–4721.

[18] Cho, J.Y.; Kim, D.; Park, Y.J.; Yang, T.Y.; Lee, Y.Y.; Joo, Y.C. The Phase-Change Kinetics of Amorphous Ge2Sb2Te5 and Device Characteristics Investigated by Thin Film Mechanics. Acta Mater. 2015, 94, 143–151.

[19] Zhao, X.L.; Zhang, X.M.; Shang, D.S.; Wu, Z.H.; Xiao, X.H.; Chen, R.; Tang, C.Y.; Liu, J.C.; Li, W.Q.; Lv, H.B.; et al. Uniform, Fast, and Reliable LixSiOy-based Resistive Switching Memory. IEEE Electron Device Lett. 2019, 40, 554–557.

[20] Guo, M.F.; Jiang, J.Y.; Qian, J.F.; Liu, C.; Ma, J.; Nan, C.W.; Shen, Y. Flexible Robust and High-Density FeRAM from Array of Organic Ferroelectric Nano-Lamellae by Self-Assembly. Adv. Sci. 2019, 6, 1801931.

[21] Qin, S.J.; Jiang, Z.Z.; Li, H.T.; Fujii, S.; Lee, D.; Wong, S.S.; Wong, H.S.P. Next-Generation Ultrahigh-Density 3-D Vertical Resistive Switching Memory (VRSM)-Part I: Accurate and Computationally Efficient Modeling. IEEE Trans. Electron Devices 2019, 66, 5139–5146.

[22] Nomura, Y.; Nomura, K.; Kinoshita, K.; Kawae, T.; Morimoto, A. Retention Properties with High-Temperature Resistance in (Bi, Pr)(Fe, Mn)O3 Thin Film Capacitor. Phys. Status Solidi (RRL) Rapid Res. Lett. 2014, 8, 536–539.

[23] Xiang, Y.C.; Huang, P.; Zhao, Y.D.; Zhao, M.R.; Gao, B.; Wu, H.Q.; Qian, H.; Liu, X.Y.; Kang, J.F. Impacts of State Instability and Retention Failure of Filamentary

Analog RRAM on the Performance of Deep Neural Network. IEEE Trans. Electron Devices 2019, 66, 4517–4522.

[24] L. Chua, "Memristor-The missing circuit element," in IEEE Transactions on Circuit Theory, vol. 18, no. 5, pp. 507-519, September 1971, doi: 10.1109/TCT.1971.1083337.

[25] Feng, Liu. “2D Photonic Memristor Beyond Graphene: Progress and Prospects.” Nanophotonics (Berlin, Germany) 9.7 (2020): 1579–1599. Web.

[26] Strukov, D., Snider, G., Stewart, D. et al. The missing memristor was found. Nature 453, 80–83 (2008). https://doi.org/10.1038/nature06932

[27] Waser, R., Dittmann, R., Staikov, G., and Szot, K. (2009). Redox-based resistive switching memories–nanoionic mechanisms, prospects, and challenges. Adv. Mater. 21, 2632–2663. doi: 10.1002/adma.200900375

[28] Lee, K. J., Cho, B. H., Cho, W. Y., Kang, S., Choi, B. G., Oh, H. R., et al. (2008). A 90 nm 1.8 V 512 Mb diode-switch PRAM with 266 MB/s read throughput. IEEE. J. Solid State Circ. 43, 150–162. doi: 10.1109/JSSC.2007.908001

[29] Wong, H. S. P., Lee, H. Y., Yu, S., Chen, Y. S., Wu, Y., Chen, P. S., et al. (2012). Metal–oxide RRAM. Proc. IEEE 100, 1951–1970. doi: 10.1109/JPROC.2012.2190369

[30] Akinaga, H., and Shima, H. (2010). Resistive random access memory (ReRAM) based on metal oxides. Proc. IEEE 98, 2237–2251. doi: 10.1109/JPROC.2010.2070830

[31] Wong, H. S. P., Lee, H. Y., Yu, S., Chen, Y. S., Wu, Y., Chen, P. S., et al. (2012). Metal–oxide RRAM. Proc. IEEE 100, 1951–1970. doi: 10.1109/JPROC.2012.2190369

[32] Yang, J. J., Strukov, D. B., and Stewart, D. R. (2013). Memristive devices for computing. Nat. Nanotechnol. 8, 13–24. doi: 10.1038/nnano.2012.240

[33] Choi, S., Yang, Y., and Lu, W. (2014). Random telegraph noise and resistance switching analysis of oxide based resistive memory. Nanoscale 6, 400–404. doi: 10.1039/C3NR05016E

[34] Sun, K., Chen, J., and Yan, X. (2020). The future of memristors: materials engineering and neural networks. Adv. Funct. Mater. 31:2006773. doi: 10.1002/adfm.202006773

[35] Wang, Z., Wu, H., Burr, G. W., Hwang, C. S., Wang, K. L., Xia, Q., et al. (2020). Resistive switching materials for information processing. Nat. Rev. Mater. 5, 173–195. doi: 10.1038/s41578-019-0159-3

[36] Zhang, Y., Wang, Z., Zhu, J., Yang, Y., Rao, M., Song, W., et al. (2020). Brain-inspired computing with memristors: challenges in devices, circuits, and systems. Appl. Phys.

Rev. 7:011308. doi: 10.1063/1.5124027

[37] Strukov, D., Snider, G., Stewart, D. et al. The missing memristor was found. Nature 453, 80–83 (2008). https://doi.org/10.1038/nature06932

[38] Tan, H.; Liu, G.; Zhu, X.; Yang, H.; Chen, B.; Chen, X.; Shang, J.; Lu, W. D.; Wu, Y.; Li, R. W. An Optoelectronic Resistive Switching Memory with Integrated Demodulating and Arithmetic Functions. Adv. Mater. 2015, 27, 2797– 2803, DOI: 10.1002/adma.201500039

[39] Leydecker, T.; Herder, M.; Pavlica, E.; Bratina, G.; Hecht, S.; Orgiu, E.; Samorì, P. Flexible Non-Volatile Optical Memory Thin-Film Transistor Device with Over 256 Distinct Levels Based on an Organic Bicomponent Blend. Nat. Nanotechnol. 2016, 11, 769– 775, DOI: 10.1038/nnano.2016.87

[40] Wang, W.; Gao, S.; Li, Y.; Yue, W.; Kan, H.; Zhang, C.; Lou, Z.; Wang, L.; Shen, G. Artificial Optoelectronic Synapses Based on TiNxO2–x/MoS2 Heterojunction for Neuromorphic Computing and Visual System. Adv. Funct. Mater. 2021, 31, 2101201, DOI: 10.1002/adfm.202101201

[41] Zhou, F.; Liu, Y.; Shen, X.; Wang, M.; Yuan, F.; Chai, Y. Low-Voltage, Optoelectronic CH3NH3PbI3–xClx Memory with Integrated Sensing and Logic Operations. Adv. Funct. Mater. 2018, 28, 1800080, DOI: 10.1002/adfm.201800080

[42] Sun K, Chen J, Yan X. The Future of Memristors: Materials Engineering and Neural Networks. Advanced functional materials. 2021;31(8):2006773-n/a. doi:10.1002/adfm.202006773

[43] Xu, W., Wang, J., & Yan, X. (2021). Advances in memristor-based neural networks. Frontiers in Nanotechnology, 3, 645995.

[44] Choi, S., Tan, S. H., Li, Z., Kim, Y., Choi, C., Chen, P. Y., et al. (2018). SiGe epitaxial memory for neuromorphic computing with reproducible high performance based on engineered dislocations. Nat. Mater. 17, 335–340. doi: 10.1038/s41563-017-0001-5

[45] Yan, X., Zhao, J., Liu, S., Zhou, Z., Liu, Q., Chen, J., et al. (2018b). Memristor with Ag-cluster-doped TiO2 films as artificial synapse for Neuroinspired computing. Adv. Funct. Mater. 28:1705320. doi: 10.1002/adfm.201705320

[46] Xia, Q., and Yang, J. J. (2019). Memristive crossbar arrays for brain-inspired computing. Nat. Mater. 18, 309–323. doi: 10.1038/s41563-019-0291-x

[47] Ou Q-F, Xiong B-S, Yu L, Wen J, Wang L, Tong Y. In-Memory Logic Operations and Neuromorphic Computing in Non-Volatile Random Access Memory. Materials. 2020; 13(16):3532. https://doi.org/10.3390/ma13163532

[48] Guo, T., Sun, B., Ranjan, S., Jiao, Y., Wei, L., Zhou, Y. N., & Wu, Y. A. (2020). From memristive materials to neural networks. ACS Applied Materials & Interfaces, 12(49),

54243-54265.

[49] Brataas A, Kent AD, Ohno H. Current-induced torques in magnetic materials. Nature materials. 2012;11(5):372-381. doi:10.1038/NMAT3311

[50] Muhammad Shahrukh Saleem, Bin Cui, Cheng Song, Yiming Sun, Youdi Gu, Ruiqi Zhang, Muhammad Umer Fayaz, Xiaofeng Zhou, Peter Werner, Stuart S. P. Parkin, and Feng Pan. Electric Field Control of Phase Transition and Tunable Resistive Switching in SrFeO2.5. ACS Applied Materials & Interfaces 2019 11 (6), 6581-6588. DOI: 10.1021/acsami.8b18251

[51] Xidi Sun, Xiaoming Mo, Lihu Liu, Huiyuan Sun, and Caofeng Pan. ACS Applied Materials & Interfaces 2019 11 (24), 21661-21667. Voltage-Driven Room-Temperature Resistance and Magnetization Switching in Ceramic TiO2/PAA Nanoporous Composite Films DOI: 10.1021/acsami.9b02593

[52] Garcia V, Bibes M. Ferroelectric tunnel junctions for information storage and processing. Nature communications. 2014;5(1):4289-4289. doi:10.1038/ncomms5289

[53] Xue F, He X, Wang Z, et al. Giant Ferroelectric Resistance Switching Controlled by a Modulatory Terminal for Low-Power Neuromorphic In-Memory Computing. Advanced materials (Weinheim). 2021;33(21):e2008709-n/a. doi:10.1002/adma.202008709

[54] Xue, F., He, X., Ma, Y. et al. Unraveling the origin of ferroelectric resistance switching through the interfacial engineering of layered ferroelectric-metal junctions. Nat Commun 12, 7291 (2021). https://doi.org/10.1038/s41467-021-27617-6

[55] E. Y. Tsymbal, A. Gruverman, V. Garcia, M. Bibes, A. Barthélémy, Ferroelectric and multiferroic tunnel junctions. MRS Bull. 37, 138–143 (2012).

[56] D. S. Jeong et al., Emerging memories: resistive switching mechanisms and current status. Rep. Prog. Phys. 75, 76502 (2012).

[57] Yan X, Zhao Q, Chen AP, et al. Vacancy-Induced Synaptic Behavior in 2D WS2 Nanosheet-Based Memristor for Low-Power Neuromorphic Computing. Small (Weinheim an der Bergstrasse, Germany). 2019;15(24):e1901423-e1901423. doi:10.1002/smll.201901423

[58] Wang C, Sun J, Ni W, et al. Tuning oxygen vacancy in $LiNbO_3$ single crystals for prominent memristive and dielectric behaviors. Journal of the American Ceramic Society. 2019;102(11):6705-6712. doi:10.1111/jace.16522

[59] Wu C, Li X, Xu X, Lee BW, Chae SC, Liu C. Self-rectifying resistance switching memory based on a dynamic p–n junction. Nanotechnology. 2021;32(8):85203-085203. doi:10.1088/1361-6528/abc782

[60] Lv F, Ling K, Wang W, et al. Multilevel resistance switching behavior in PbTiO3/Nb:SrTiO3(100) heterostructure films grown by hydrothermal epitaxy. Journal of alloys and compounds. 2019;778:768-773. doi:10.1016/j.jallcom.2018.11.118

[61] M. A. Zidan, J. P. Strachan, and W. D. Lu, “The future of electronics based on memristive systems,” Nature Electron., vol. 1, no. 1, pp. 22–29, Jan. 2018

[62]] S. B. Eryilmaz, D. Kuzum, S. Yu, and H.-S.-P. Wong, “Device and system level design considerations for analog-non-volatile-memory based neuromorphic architectures,” in IEDM Tech. Dig., Dec. 2015, pp. 4.1.1–4.1.4.

[63] D. Lee et al., “Oxide based nanoscale analog synapse device for neural signal recognition system,” in IEDM Tech. Dig., Dec. 2015, pp. 4.7.1–4.7.4.

[64] P. Yao et al., “Face classification using electronic synapses,” Nature Commun., vol. 8, no. 1, Aug. 2017, Art. no. 15199.

[65] M. Prezioso, F. Merrikh-Bayat, B. D. Hoskins, G. C. Adam, K. K. Likharev, and D. B. Strukov, “Training and operation of an integrated neuromorphic network based on metal-oxide memristors,” Nature, vol. 521, pp. 61–64, Dec. 2015.

[66] S. Yu, B. Gao, Z. Fang, H. Yu, J. Kang, and H.-S. P. Wong, “A low energy oxide-based electronic synaptic device for neuromorphic visual systems with tolerance to device variation,” Adv. Mater., vol. 25, pp. 1774–1779, Mar. 2013, doi: 10.1002/adma.201203680.

[67] I. Hubara, M. Courbariaux, D. Soudry, R. El-Yaniv, and Y. Bengio, “Quantized neural networks: Training neural networks with low precision weights and activations,” 2016, arXiv:1609.07061.

[68] K. Ando et al., “BRein memory: A single-chip binary/ternary reconfigurable in-memory deep neural network accelerator achieving 1.4 Tops at 0.6 W,” IEEE J. Solid-State Circuits, vol. 53, no. 4, pp. 983–994, Apr. 2018.

[69] H. Valavi, P. J. Ramadge, E. Nestler, and N. Verma, “A 64-Tile 2.4-Mb in-memory-computing CNN accelerator employing charge-domain compute,” IEEE J. Solid-State Circuits, vol. 54, no. 6, pp. 1789–1799, Jun. 2019.

[70] S. K. Gonugondla, M. Kang, and N. Shanbhag, “A 42pJ/decision 3.12TOPS/W robust in-memory machine learning classifier with on-chip training,” in IEEE Int. Solid-State Circuits Conf. (ISSCC) Dig. Tech. Papers, Feb. 2018, pp. 490–492.

[71] J.-M. Hung, C.-J. Jhang, P.-C. Wu, Y.-C. Chiu, and M.-F. Chang, “Challenges and trends of nonvolatile in-memory-computation circuits for AI edge devices,” IEEE Open J. Solid-State Circuits Soc., vol. 1, pp. 171–183, 2021.

[72] Sien Ng, Rohit Abraham John, Jing-ting Yang, and Nripan Mathews. Forming-Less

Compliance-Free Multistate Memristors as Synaptic Connections for Brain-Inspired Computing. ACS Applied Electronic Materials 2020 2 (3), 817-826 DOI: 10.1021/acsaelm.0c00002

[73] N. Vasileiadis, P. Dimitrakis, V. Ntinas and G. C. Sirakoulis, "True Random Number Generator Based on Multi-State Silicon Nitride Memristor Entropy Sources Combination," 2021 International Conference on Electronics, Information, and Communication (ICEIC), Jeju, Korea (South), 2021, pp. 1-4, doi: 10.1109/ICEIC51217.2021.9369817.

[74] Zhang, H., Zhao, H., Wang, M., Xiao, Y., Zhao, D., & Liu, R. (2022). Research Progress on Novel Structures of Flexible Memristor Devices. Interdisciplinary Research for Printing and Packaging, 518-522.

[75] R. Li et al., "Thermal-Induced Multi-State Memristors for Neuromorphic Engineering," 2023 IEEE International Symposium on Circuits and Systems (ISCAS), Monterey, CA, USA, 2023, pp. 1-5, doi: 10.1109/ISCAS46773.2023.10182122.

[76] Li, Y., Wang, Z., Midya, R., Xia, Q., & Yang, J. J. (2018). Review of memristor devices in neuromorphic computing: materials sciences and device challenges. Journal of Physics D: Applied Physics, 51(50), 503002.

[77] Han, J. W., & Meyyappan, M. (2011). Copper oxide resistive switching memory for e-textile. AIP Advances, 1(3).

[78] Wu, Y., Lee, B., & Wong, H. S. P. (2010). Al2O3 Based RRAM Using Atomic Layer Deposition (ALD) With 1-uA RESET Current. IEEE electron device letters, 31(12), 1449-1451.

[79] Shih, A., Zhou, W., Qiu, J., Yang, H. J., Chen, S., Mi, Z., & Shih, I. (2010). Highly stable resistive switching on monocrystalline ZnO. Nanotechnology, 21(12), 125201.

[80] Ma, G., Tang, X., Su, H., Li, Y., Zhang, H., & Zhong, Z. (2014). Effects of standard free energy on NiO bipolar resistive switching devices. IEEE Transactions on Electron Devices, 61(5), 1237-1240.

[81] Lv, H., & Tang, T. (2010). The Role of CuAlO Interface Layer for Switching Behavior of Al/ /Cu Memory Device. IEEE electron device letters, 31(12), 1464-1466.

[82] Li, Y., Wang, Z., Midya, R., Xia, Q., & Yang, J. J. (2018). Review of memristor devices in neuromorphic computing: materials sciences and device challenges. Journal of Physics D: Applied Physics, 51(50), 503002.

[83] Coleman, V. A., Bradby, J. E., Jagadish, C., Munroe, P., Heo, Y. W., Pearton, S. J., ... & Yano, M. (2005). Mechanical properties of ZnO epitaxial layers grown on a-and c-axis sapphire. Applied Physics Letters, 86(20).

[84] Lin, C.; Tang, C.; Wu, S.-C.; Yang, S.; Lai, Y.; Wu, S. Resistive Switching

Characteristics of Zinc Oxide (ZnO) Resistive RAM with Al Metal Electrode. In Proceedings of the 4th IEEE International NanoElectronics Conference, Tao-Yuan, Taiwan, 21–24 June 2011; pp. 1–2.

[85] Xue, Q.; Hang, T.; Gong, Z.; Chen, L.; Liang, J.; Sun, Y.; Lu, D.; Zhang, X.; Chen, C.C.; Li, M. Transient and Biocompatible Resistive Switching Memory Based on Electrochemically-Deposited Zinc Oxide. Adv. Electron. Mater. 2021, 7, 2100322.

[86] Tian, R.; Li, L.; Yang, K.; Yang, Z.; Wang, H.; Pan, P.; He, J.; Zhao, J.; Zhou, B. Resistance Switching Characteristics of Ag/ZnO/Graphene Resistive Random Access Memory. Vacuum 2023, 207, 111625.

[87] Sun, Y.; Yan, X.; Zheng, X.; Li, Y.; Liu, Y.; Shen, Y.; Ding, Y.; Zhang, Y. Effect of Carrier Screening on ZnO-Based Resistive Switching Memory Devices. Nano Res. 2017, 10, 77–86.

[88] Misra, P.; Das, A.K.; Kukreja, L.M. Switching Characteristics of ZnO Based Transparent Resistive Random Access Memory Devices Grown by Pulsed Laser Deposition. Phys. Status Solidi (C) Curr. Top. Solid State Phys. 2010, 7, 1718–1720.

[89] Smirnov, V.A.; Tominov, R.V.; Avilov, V.I.; Alyabieva, N.I.; Vakulov, Z.E.; Zamburg, E.G.; Khakhulin, D.A.; Ageev, O.A. Investigation into the Memristor Effect in Nanocrystalline ZnO Films. Semiconductors 2019, 53, 72–77.

[90] Delfag, M.; Rachovitis, G.; González, Y.; Jehn, J.; Youssef, A.H.; Schindler, C.; Ruediger, A. Fully Printed ZnO-Based Valency-Change Memories for Flexible and Transparent Applications. Flex. Print. Electron. 2022, 7, 045001.

[91] Xu, N.; Liu, L.; Sun, X.; Liu, X.; Han, D.; Wang, Y.; Han, R.; Kang, J.; Yu, B. Characteristics and Mechanism of Conduction/Set Process in TiN/ZnO/Pt Resistance Switching Random-Access Memories. Appl. Phys. Lett. 2008, 92, 35–38.

[92] Lin, C.-L.; Wu, S.-C.; Tang, C.C.; Lai, Y.-H.; Yang, S.-R.; Wu, S.-C. Unipolar Resistive Switching and Retention of RTA-Treated Zinc Oxide (ZnO) Resistive RAM. In Proceedings of the 18th IEEE International Symposium on the Physical and Failure Analysis of Integrated Circuits (IPFA), Incheon, Republic of Korea, 4–7 July 2011; pp. 1–5.

[93] Shih, C.C.; Chang, K.C.; Chang, T.C.; Tsai, T.M.; Zhang, R.; Chen, J.H.; Chen, K.H.; Young, T.F.; Chen, H.L.; Lou, J.C.; et al. Resistive Switching Modification by Ultraviolet Illumination in Transparent Electrode Resistive Random Access Memory. IEEE Electron Device Lett. 2014, 35, 633–635.

[94] Shih, C.C.; Chang, K.C.; Chang, T.C.; Tsai, T.M.; Zhang, R.; Chen, J.H.; Chen, K.H.; Young, T.F.; Chen, H.L.; Lou, J.C.; et al. Resistive Switching Modification by Ultraviolet Illumination in Transparent Electrode Resistive Random Access Memory.

IEEE Electron Device Lett. 2014, 35, 633–635.

[95] Kim, S.; Moon, H.; Gupta, D.; Yoo, S.; Choi, Y.K. Resistive Switching Characteristics of Sol-Gel Zinc Oxide Films for Flexible Memory Applications. IEEE Trans. Electron Devices 2009, 56, 696–699.

[96] You, H.C.; Lin, G.K. Solution-Processed ZnO Thin Films for Low Voltage and Low Temperature Application in Flexible Resistive Random Access Memory. Thin Solid Films 2016, 616, 728–732.

[97] Deshpande, S.; Nair, V.V. Resistive Switching of Al/Sol-Gel ZnO/Al Devices for Resistive Random Access Memory Applications. In Proceedings of the ACT 2009—International Conference on Advances in Computing, Control and Telecommunication Technologies, Trivandrum, India, 28–29 December 2009; pp. 471–473.

[98] Wu, C.C.; You, H.C.; Lin, Y.H.; Yang, C.J.; Hsiao, Y.P.; Liao, T.P.; Yang, W.L. Impact of Electrode Surface Morphology in ZnO-Based Resistive Random Accessmemory Fabricated Using the Cu Chemical Displacement Technique. Materials 2018, 11, 265.

[99] Fuzhen Wang, Junwei Wu, Chapter 8 - Magnetron sputtering, Editor(s): Fuzhen Wang, Junwei Wu, Modern Ion Plating Technology, Elsevier, 2023, Pages 189-228, https://doi.org/10.1016/B978-0-323-90833-7.00008-5.

[100] Xiao, X., Hu, J., Tang, S., Yan, K., Gao, B., Chen, H., & Zou, D. (2020). Recent advances in halide perovskite memristors: materials, structures, mechanisms, and applications. Advanced Materials Technologies, 5(6), 1900914.

[101] Li, Wang, Z., Midya, R., Xia, Q., & Yang, J. J. (2018). Review of memristor devices in neuromorphic computing: materials sciences and device challenges. Journal of Physics. D, Applied Physics, 51(50), 503002–. https://doi.org/10.1088/1361-6463/aade3f

[102] Hruska, J. Intel, Micron reveal Xpoint, a new memory architecture that could outclass DDR4 and NAND. ExtremeTech https://www.extremetech.com/ extreme/211087-intel-micron-reveal-xpoint-anew-memory-architecture-that- claims-tooutclass-both- ddr4-and- nand (2015).

[103] Fong, S. W., Neumann, C. M. & Wong, H.-S. P. Phasechange memory — towards a storage- class memory. IEEE Trans. Electron Devices 64, 4374–4385 (2017).

[104] Wuttig, M. Towards a universal memory. Nat. Mater. 4, 265–266 (2005).

[105] Rao, F. et al. Reducing the stochasticity of crystal nucleation to enable subnanosecond memory writing. Science 358, 1423–1427 (2017).

[106] Salinga, M. et al. Monatomic phase change memory. Nat. Mater. 17, 681–685 (2018).

[107] Fong, S. W., Neumann, C. M. & Wong, H.-S. P. Phase change memory — towards a

storage- class memory. IEEE Trans. Electron Devices 64, 4374–4385 (2017).

[108] Zhang, W., Mazzarello, R., Wuttig, M. et al. Designing crystallization in phase-change materials for universal memory and neuro-inspired computing. Nat Rev Mater 4, 150–168 (2019). https://doi-org.proxy.lib.uwaterloo.ca/10.1038/s41578-018-0076-x

[109] Wong, H.-S. P. et al. Phase change memory. Proc. IEEE 98, 2201 (2010).

[110] Raoux, S., Welnic, W. & Ielmini, D. Phase change materials and their application to nonvolatile memories. Chem. Rev. 110, 240–267 (2010).

[111] Raoux, S. & Wuttig, M. (eds) Phase Change Materials: Science and Applications (Springer US, 2008).

[112] Joshi, V., Le Gallo, M., Haefeli, S. et al. Accurate deep neural network inference using computational phase-change memory. Nat Commun 11, 2473 (2020). https://doi.org/10.1038/s41467-020-16108-9

[113] Sun, L., Zhou, YX., Wang, XD. et al. Ab initio molecular dynamics and materials design for embedded phase-change memory. npj Comput Mater 7, 29 (2021). https://doi.org/10.1038/s41524-021-00496-7

[114] Sun Z, Zhou J, Ahuja R. Structure of phase change materials for data storage. Physical review letters. 2006 Feb 9;96(5):055507.

[115] Lencer D, Salinga M, Grabowski B, Hickel T, Neugebauer J, Wuttig M. A map for phase-change materials. Nature materials. 2008 Dec;7(12):972-7.

[116] Salinga M, Kersting B, Ronneberger I, Jonnalagadda VP, Vu XT, Le Gallo M, Giannopoulos I, Cojocaru-Mirédin O, Mazzarello R, Sebastian A. Monatomic phase change memory. Nature materials. 2018 Aug;17(8):681-5.

[117] Xu M, Li B, Xu K, Tong H, Cheng X, Xu M, Miao X. Stabilizing amorphous Sb by adding alien seeds for durable memory materials. Physical Chemistry Chemical Physics. 2019;21(8):4494-500.

[118] Wang G, Shi H, Lotnyk A, Shi D, Wang R. Conversion of p–n conduction type by spinodal decomposition in Zn-Sb-Bi phase-change alloys. NPG asia Materials. 2020 Dec;12(1):17.

[119] Matsunaga T, Akola J, Kohara S, Honma T, Kobayashi K, Ikenaga E, Jones RO, Yamada N, Takata M, Kojima R. From local structure to nanosecond recrystallization dynamics in AgInSbTe phase-change materials. Nature materials. 2011 Feb;10(2):129-34.

[120] Rao F, Ding K, Zhou Y, Zheng Y, Xia M, Lv S, Song Z, Feng S, Ronneberger I, Mazzarello R, Zhang W. Reducing the stochasticity of crystal nucleation to enable subnanosecond memory writing. Science. 2017 Dec 15;358(6369):1423-7.

[121] Loke D, Lee TH, Wang WJ, Shi LP, Zhao R, Yeo YC, Chong TC, Elliott SR. Breaking the speed limits of phase-change memory. Science. 2012 Jun 22;336(6088):1566-9.

[122] Li Z, Si C, Zhou J, Xu H, Sun Z. Yttrium-doped Sb2Te3: a promising material for phase-change memory. ACS Applied Materials & Interfaces. 2016 Oct 5;8(39):26126-34.

[123] B.S. Sa, J. Zhou, Z.T. Song, Z.M. Sun, R. Ahuja. Pressure-induced topological insulating behavior in the ternary chalcogenide Ge2Sb2Te5. Phys. Rev. B, 84 (2011), p. 5

[124] G. Wang, J. Zhou, S.R. Elliott, Z. Sun. Role of carbon-rings in polycrystalline GeSb2Te4 phase-change material. J. Alloy. Compd., 782 (2019), pp. 852-858

[125] S. He, L. Zhu, J. Zhou, Z. Sun. Metastable Stacking-Polymorphism in Ge2Sb2Te5. Inorg. Chem., 56 (2017), pp. 11990-11997

[126] T. Guo, S. Song, Z. Song, X. Ji, Y. Xue, L. Chen, Y. Cheng, B. Liu, L. Wu, M. Qi, S. Feng. SiC-Doped Ge2Sb2Te5 phase-change material: a candidate for high-density embedded memory application.Adv. Electron. Mater., 4 (2018)

[127] R. Li, Y.H. Guo, B. Xu, Y. Su, J. Yin, C.H. Zhang, Y.D. Xia, Z.G. Liu, Z. Xu, L.C. Wu, Z.T. Song. Experimental and theoretical investigations on effects of hydrostatic pressure on the electrical properties of rhombohedral Sb2Te3. AIP Adv., 1 (2011)

[128] F. Rao, Z. Song, M. Zhong, L. Wu, G. Feng, B. Liu, S. Feng, B. Chen. Multilevel Data Storage Characteristics of Phase Change Memory Cell with Doublelayer Chalcogenide Films (Ge2Sb2Te5 and Sb2Te3).Jpn. J. Appl. Phys., 46 (2007), pp. L25-L27

[129] M. Zhu, L. Wu, F. Rao, Z. Song, K. Ren, X. Ji, S. Song, D. Yao, S. Feng. Uniform Ti-doped Sb2Te3 materials for high-speed phase change memory applications. Appl. Phys. Lett., 104 (2014), Article 053119

[130] Z. Li, C. Si, J. Zhou, H.B. Xu, Z.M. Sun. Yttrium-doped Sb2Te3: a promising material for phase-change memory. ACS Appl. Mater. Interfaces, 8 (2016), pp. 26126-26134

[131] Zhang, W., Mazzarello, R., Wuttig, M. et al. Designing crystallization in phase-change materials for universal memory and neuro-inspired computing. Nat Rev Mater 4, 150–168 (2019). https://doi.org/10.1038/s41578-018-0076-x

[132] Wang, Q., Lei, Y., Wang, Y., Liu, Y., Song, C., Zeng, J., ... & Li, Y. (2020). Atomic-scale engineering of chemical-vapor-deposition-grown 2D transition metal dichalcogenides for electrocatalysis. Energy & Environmental Science, 13(6), 1593-1616.

[133] Binnewies M, Glaum R, Schmidt M, Schmidt P. Chemical vapor transport reactions.

Walter de Gruyter; 2012 Aug 31.

[134] Binnewies M, Glaum R, Schmidt M, Schmidt P. Chemical vapor transport reactions–a historical review. Zeitschrift für anorganische und allgemeine Chemie. 2013 Feb;639(2):219-29.

[135] Lenz M, Gruehn R. Developments in measuring and calculating chemical vapor transport phenomena demonstrated on Cr, Mo, W, and their compounds. Chemical reviews. 1997 Dec 18;97(8):2967-94.

[136] Nandakumar, S.R., Boybat, I., Le Gallo, M. et al. Experimental Demonstration of Supervised Learning in Spiking Neural Networks with Phase-Change Memory Synapses. Sci Rep 10, 8080 (2020). https://doi.org/10.1038/s41598-020-64878-5

[137] Yang Ren, Ping Liu, Rongxin Liu, Yunwei Wang, Yubin Wei, Lihua Jin, Gaoyang Zhao, The key of ITO films with high transparency and conductivity: Grain size and surface chemical composition, Journal of Alloys and Compounds, Volume 893, 2022, 162304, ISSN 0925-8388, https://doi.org/10.1016/j.jallcom.2021.162304.

[138] Bindu, P., Thomas, S. Estimation of lattice strain in ZnO nanoparticles: X-ray peak profile analysis. J Theor Appl Phys 8, 123–134 (2014). https://doi.org/10.1007/s40094-014-0141-9

[139] Kotsis K, Staemmler V. Ab initio calculations of the O1s XPS spectra of ZnO and Zn oxo compounds. Physical chemistry chemical physics : PCCP. 2006;8(13):1490-1498. doi:10.1039/b515699h

[140] Biolek D, Biolek Z, Biolková V. Interpreting area of pinched memristor hysteresis loop. Electronics letters. 2014;50(2):74-75. doi:10.1049/el.2013.3108

[141] Liu B, Li H, Chen Y, Li X, Wu Q, Huang T. Vortex: variation-aware training for memristor X-bar. In: 2015 52nd ACM/EDAC/IEEE Design Automation Conference (DAC). Vol 2015-. ACM; 2015:1-6. doi:10.1145/2744769.2744930

[142] Guo, T., Zhang, B., Wang, X., Xiao, Y., Sun, B., Zhou, Y. N., & Wu, Y. A. (2023). Broadband Optoelectronic Synapse Enables Compact Monolithic Neuromorphic Machine Vision for Information Processing. Advanced Functional Materials, 2303879.

[143] Emtage PR, Tantraporn W. Schottky emission through thin insulating films. Physical review letters. 1962;8(7):267-268. doi:10.1103/PhysRevLett.8.267

[144] Dittmann, R., Menzel, S., & Waser, R. (2021). Nanoionic memristive phenomena in metal oxides: the valence change mechanism. Advances in physics, 70(2), 155-349.

[145] Prezioso M, Riminucci A, Graziosi P, et al. A Single-Device Universal Logic Gate Based on a Magnetically Enhanced Memristor. Advanced materials (Weinheim). 2013;25(4):534-538. doi:10.1002/adma.201202031

[146] Im HJ, Koo B, Kim MS, Lee JE. Solvothermal synthesis of Sb2Te3 nanoplates under

various synthetic conditions and their thermoelectric properties. Applied surface science. 2019;475:510-514. doi:10.1016/j.apsusc.2019.01.014

[147] Boschker, J., Galves, L., Flissikowski, T. et al. Coincident-site lattice matching during van der Waals epitaxy. Sci Rep 5, 18079 (2016). https://doi.org/10.1038/srep18079